



## NISTIR 5900

---

---

# Multi-Scale Picture of Concrete and its Transport Properties: Introduction for Non-Cement Researchers

---

---

Edward J. Garboczi and Dale P. Bentz



Building and Fire Research Laboratory  
Gaithersburg, Maryland 20899

**NIST**

QC  
100  
.U56  
NO. 5900  
1996

United States Department of Commerce  
Technology Administration  
National Institute of Standards and Technology



# Multi-Scale Picture of Concrete and its Transport Properties: Introduction for Non-Cement Researchers

---

---

Edward J. Garboczi and Dale P. Bentz

October 1996  
Building and Fire Research Laboratory  
National Institute of Standards and Technology  
Gaithersburg, Maryland 20899



**U.S. Department of Commerce**  
Michael Kantor, *Secretary*  
**Technology Administration**  
Mary L. Good, *Under Secretary for Technology*  
National Institute of Standards and Technology  
Arati Prabhakar, *Director*



# ABSTRACT

Concrete is a multi-length scale composite material. From the nanometer to the millimeter scale, it is a random composite, and a different random composite at each length scale. Percolation processes play a key role in the microstructure of concrete, and help to describe the overall dependence of transport properties like ionic diffusivity on the microstructure. Computer models have been developed to describe the microstructure and transport properties, as the randomness of the material precludes most (but not all) analytical formulations. The overall description of concrete, over six orders of magnitude of length scales, in terms of computer models, percolation theory, and composite ideas is of interest to those studying other random materials as well, like ceramics and rocks. This report is written to present the ideas for concrete in such a way so as to be accessible to the non-cement researcher. It is hoped that these ideas will prove to be useful in other materials.

**Keywords:** Building technology, cement paste, computer modelling, concrete, microstructure, mortar, percolation, transport properties.

*Cover picture, from left to right: transmission electron micrograph of C-S-H phase of cement paste (300 x 300nm), scanning electron micrograph of cement paste (300 x 300μm), and optical micrograph of concrete (30 x 30mm)*



# Contents

<b>Abstract</b>	<b>iii</b>
<b>List of Figures</b>	<b>vii</b>
<b>Executive Summary</b>	<b>ix</b>
<b>1 Introduction</b>	<b>1</b>
1.1 The history and importance of concrete . . . . .	1
1.2 The complexity of concrete microstructure . . . . .	2
<b>2 Basic Concepts</b>	<b>3</b>
<b>3 Cement Paste</b>	<b>5</b>
3.1 Solids percolation: set point . . . . .	11
3.2 Capillary pore space percolation . . . . .	14
3.3 C-S-H percolation . . . . .	16
3.4 Cement paste pore size . . . . .	18
3.5 Diffusivity of Cement Paste . . . . .	18
3.6 CH percolation: Leaching . . . . .	20
<b>4 Microstructure of Mortar and Concrete</b>	<b>21</b>
4.1 Interfacial Zone Microstructure . . . . .	22
4.2 Concrete considered as a composite material . . . . .	23
4.3 Interfacial Zone Percolation . . . . .	24
4.4 Diffusivity/conductivity of concrete . . . . .	31
<b>5 C-S-H</b>	<b>35</b>
<b>6 Multiscale models for the ionic diffusivity</b>	<b>37</b>
<b>7 Summary</b>	<b>39</b>
<b>8 Acknowledgements</b>	<b>40</b>
<b>9 References</b>	<b>41</b>



## List of Figures

1	Showing concrete at four different length scales: upper left is concrete, upper right is mortar, lower left is cement paste, lower right is C-S-H. . . . .	3
2	Showing processed and segmented SEM images of four kinds of portland cement particles. Each phase in the cement is identified by a unique color. The random microstructural differences between particles in the same cement, and between particles in different cements, is readily apparent. . . . .	7
3	Showing four stages of hydration in a microstructural model of C3S hydration. The degrees of hydration are: top left-0, top right-20 %, bottom left-50%, bottom right-87%. Red=unreacted cement, blue=CH, yellow=C-S-H, and black= porosity. . . . .	11
4	Showing the capillary porosity remaining at the set point, for several experimental and model cement pastes involving different initial cement particle configurations, as a function of the w/c ratio of the cement paste. . . . .	13
5	Showing the fraction of the capillary pore space that is part of a percolated (continuous) cluster, for several different w/c cement pastes as a function of degree of hydration. . . . .	15
6	Showing the fraction of the capillary pore space that is part of a percolated (continuous) cluster, for several different w/c cement pastes as a function of capillary porosity. . . . .	16
7	Showing the electrical conductivity of the cement paste at $-40^{\circ}$ , plotted vs. the volume fraction of C-S-H. The solid symbols are model results, and the open symbols represent experimental values. . . . .	17
8	Showing cement paste conductivity results, normalized by the pore fluid conductivity, for an 0.5 w/c cement paste as a function of the capillary porosity. . . . .	19
9	Showing model data for the diffusivity for several different w/c cement pastes, normalized by the free water diffusivity, all plotted vs. capillary porosity. . . . .	20
10	Showing experimental and model results for how the relative diffusivity changes as the amount of CH leached away increases. . . . .	22
11	Showing a slice of a three dimensional model of mortar, with four aggregate diameters ranging between 0.5mm and 3mm. The four colors (dark blue, light blue, green, and red, indicate, from small to large, the four aggregate sizes used. The interfacial transition zone is shown as yellow. . . . .	25
12	Showing slices of two different three dimensional concrete models, with spherical and ellipsoidal shaped aggregate particles. Aggregates are white, bulk cement paste is gray, and the interfacial transition zones are black. . . . .	27
13	Showing the volume fractions of the hard cores and the soft shells when the soft shell phase has just percolated, for monosize spherical hard core particless. The solid lines are from an effective medium theory described later in the text. . . . .	29
14	Showing the fraction of the total interfacial zone volume that is a part of a percolated (continuous) cluster as a function of aggregate volume fraction and for several interfacial zone thicknesses. . . . .	30

15	Showing the fraction of the total cement paste volume fraction that lies within a given distance from an aggregate surface, for a mortar with a sand volume fraction of 0.552, and a concrete with an aggregate volume fraction of 0.646.	31
16	The exact initial slope of the conductivity, in the limit of dilute sand concentration, is shown as a function of $\sigma_s/\sigma_p$ for the four size model mortar. . . .	33
17	Composite conductivity for the four size model mortar is plotted vs. the interfacial zone conductivity. [Both are normalized by bulk paste conductivity.] The solid dots are the random walk data; also shown are the effective medium results (SC=self consistent and D=differential). . . . .	34
18	Composite conductivities (calculated by random walk simulations) for the random model are shown as a function of sand concentration for three values of the interfacial zone conductivity. Also shown are the predictions of the SC and D-EMT calculations, with the same normalization as in the previous figure.	36
19	The exact initial slope of the conductivity, in the limit of dilute sand concentration, is shown as a function of $\sigma_s/\sigma_p$ for a typical mortar and a typical concrete aggregate particle size distribution. . . . .	37
20	Two-dimensional slices from three-dimensional model microstructures of the C-S-H gel at the scale of nanometers. The left image is of the micro model (25 nm by 25 nm), and the right image is of the macro model (250 nm by 250 nm). White=solid, black=pore. . . . .	38

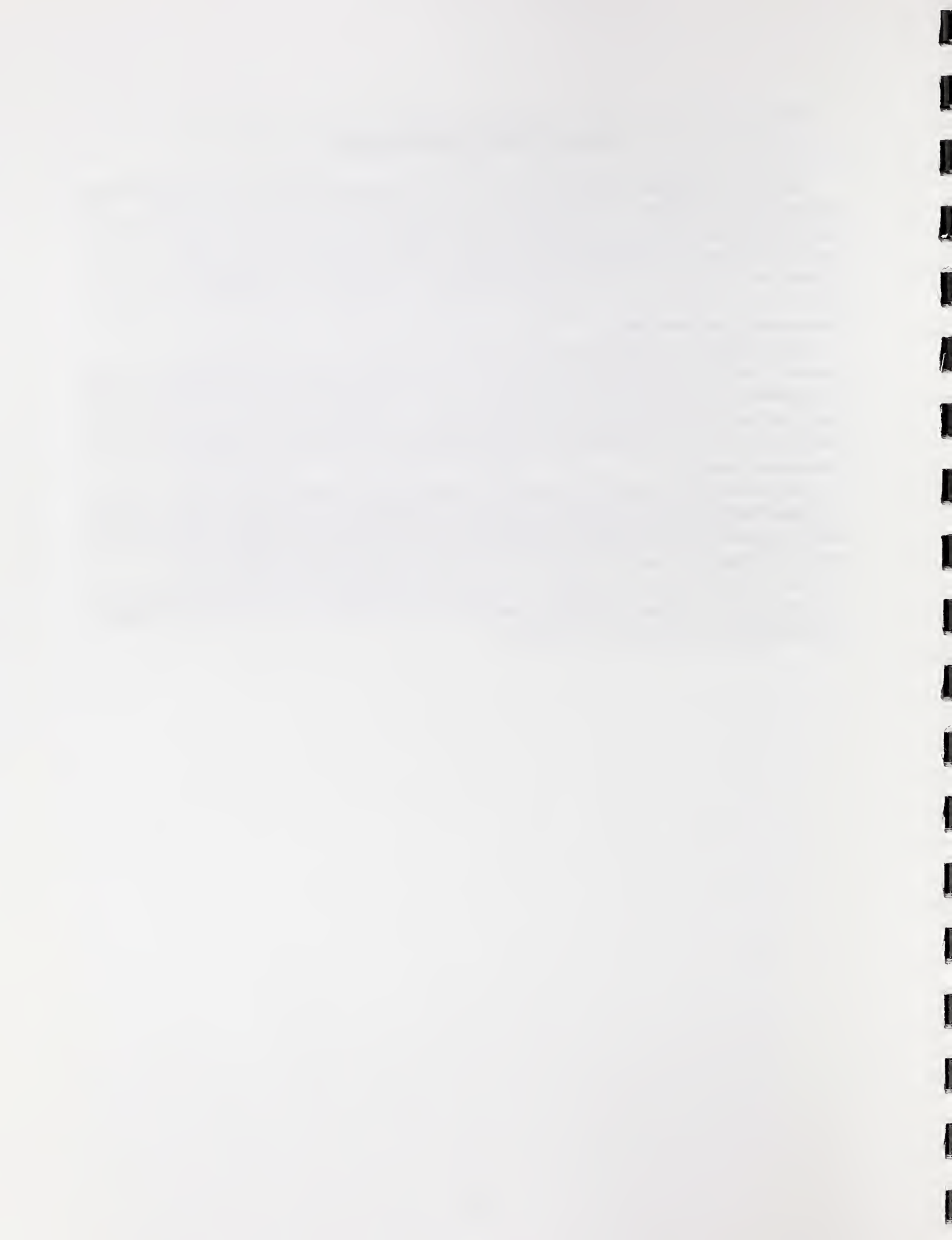
## EXECUTIVE SUMMARY

Concrete is a complex composite material. It has random microstructure at length scales ranging from nanometers to millimeters. The calcium silicate gel phase is a random composite at the nanometer scale, cement paste has complex microstructure at the micrometer scale, and the random arrangement of aggregates (rocks, sand) in concrete makes it a random composite at the millimeter scale. This multi-length scale, random microstructure can be approximately described using computer models, whose results are interpreted via percolation theory and composite theory.

First concrete and percolation theory ideas are introduced. Cement paste, at the micrometer scale, is then considered. The basic digital-image-based cement hydration model is introduced. Percolation ideas are then applied to understand model and experimental results for the set point (solids percolation), capillary pore space percolation, calcium silicate gel percolation, cement paste pore size, cement paste diffusivity, and calcium hydroxide percolation (leaching).

Next, the microstructure of mortar and concrete is considered, using the hard core/soft shell percolation model. The percolation of the interfacial transition zone phase is studied, and its importance to the transport properties of concrete explained. Using these percolation ideas, the diffusivity/conductivity of concrete can be approximately mapped out.

Finally, after presenting a computer model for the nanostructure of calcium silicate gel, and studying its transport properties, the elements of a multi-scale model for the diffusivity/conductivity of concrete are presented.



# 1 Introduction

## 1.1 The history and importance of concrete

The Romans first invented what today we call hydraulic cement-based concrete. They built numerous concrete structures, including the Pantheon in Rome, one of the finest examples of Roman architecture that survives to this day, which has a 42-meter-diameter dome made of poured concrete [1]. The name concrete comes from the Latin "concretus", which means to grow together. This is a good name for this material, as the chemical hydration process, which mainly occurs over the time scale of hours and days, causes the material to grow together from a viscoelastic, moldable liquid into a hard, rigid solid. In our world today, concrete has become ubiquitous, and in fact it is hard to imagine modern life without it. More than five trillion kilograms of concrete are used around the world each year, enough for about one thousand kilograms for each person per year, at a volume of about 400L per person. The cement used mostly in today's concrete is called portland cement. The process to produce portland cement was invented by Joseph Aspdin in the early 1800's in England. The name portland may have been originally a marketing ploy, as portland building stone was very popular in England at that time [1], and Aspdin may have wanted people to favorably compare concrete made with his cement to the popular building stone.

It is important to remember that cement is the powder that reacts with water to form cement paste, a hard, solid material that forms the matrix for the concrete composite. The addition of sand (fine aggregates) that are up to a few millimeters in diameter makes mortar, and the addition of rocks (coarse aggregates) of up to a few centimeters in diameter makes concrete. It has always been known that concrete is a porous material, whose properties depend on its pore space. There are many different kinds of pores in concrete, ranging from the air voids that are entrapped in the mixing process, which can be quite large, up to a few millimeters in diameter, to the capillary pores, which are essentially the space occupied by the leftover water from mixing, down to the nanometer-scale pores that exist in some of the hydration products produced by the cement-water chemical reaction.

Until recent years, the overwhelming focus has been on concrete's compressive strength, which has been mainly related to the overall porosity of the cement paste matrix and the amount and structure of the aggregates. Mechanical strength depends on defects and not on any overall average property, and so is very difficult to relate to microstructure. This has caused relatively little attention to be paid to the details of the pore space. Unfortunately, it has perhaps led to the idea that concrete is simply a commodity material, with nothing needed to be understood about the microstructure. However, more recently, it has been recognized that much of the concrete in the infrastructure in the U.S. and Europe and elsewhere has been deteriorating faster than expected, with much of this deterioration due to the corrosion of reinforcing steel coming from the ingress of chloride and other ions from road salts, marine environments, and ground soils. Hence close attention is now being paid to the transport properties of concrete (diffusivity, permeability, sorptivity, etc.) which, although still difficult to relate to pore structure and microstructure, are easier to study in a fundamental way than is compressive strength [2]. This has led to new attention being paid to the microstructure of concrete, with the realization that concrete is a complex composite, whose improvement and control require the usual materials science approach of processing,

microstructure, and properties.

This chapter briefly reviews some of the main ideas that have been proposed and partially validated to attempt to explain the microstructure of concrete and its effect on transport properties. The main ideas used are percolation and composite theory, combined with quantitative computer simulations. This chapter reflects the authors' view of concrete microstructure, and draws heavily on computer simulations of the microstructure. Not every part of this view has been validated experimentally, though much has, so that we expect some parts to change over time as new experiments (and new simulations!) are performed.

## 1.2 The complexity of concrete microstructure

Concrete is a composite material whose microstructure contains random features over a wide range of length scales, from nanometers to millimeters, with each length scale presenting a new random composite with which to deal [3]. In its actual uses, at the length scale of meters, concrete (almost always reinforced by steel) is usually considered to be a uniform material, with bulk properties like compressive strength, creep, and others. This is the usual engineering length scale.

Figure 1 shows four microscopic views of concrete, displaying the length scales of the material itself. In the upper left of the figure, there is an optical micrograph of concrete. The bars at the bottom of this image are millimeter bars. At this length scale, the concrete can be considered to be a mortar-large aggregate random composite, where the large aggregates range from 3mm to 30mm. The top right image shows a magnified optical micrograph of a piece of the matrix phase from the previous image, where now the mortar is itself seen to be a cement paste-sand composite. The bars at the bottom of the image are again millimeters. The size of the aggregates in this image range from a millimeter or so down to a few tenths of a millimeter. Looking closely at the matrix of the mortar composite, dark specks can be seen, of the order of tens of micrometers. These are pieces of unhydrated cement.

Turning to the lower left image in Fig. 1, we see a backscattered electron scanning electron micrograph of the cement paste matrix. The large white clumps are the largest of the unreacted cement grains, with the largest grains in the image being about  $50\mu\text{m}$  to  $80\mu\text{m}$ . These were seen as small dark specks in the previous mortar image. The contrast in a backscattered electron scanning electron micrograph is provided by average atomic number, and so the unreacted cement grains are now the brightest phase. Cement paste is clearly a random composite material, made up of unreacted cement, capillary pores, and various other chemical phases that are a result of the hydration reactions between water and cement [4]. The main reaction product phase is an amorphous or at best poorly crystalline calcium silicate hydrate gel, produced via a hydration reaction and denoted C-S-H (in cement chemistry notation,  $\text{C}=\text{CaO}$ ,  $\text{H}=\text{H}_2\text{O}$ ,  $\text{S}=\text{SiO}_2$ ,  $\text{F}=\text{Fe}_2\text{O}_3$ ,  $\text{A}=\text{Al}_2\text{O}_3$ ,  $\text{S}=\text{SO}_3$ ). This is really the glue that holds the cement paste together, just as cement paste is the glue that holds mortar and concrete together. In the image, this is the gray that lines the cement grains and is clumped in between, showing where small cement grains used to be before being consumed by the hydration reaction. The randomness in the cement paste microstructure is on the order of micrometers, because the original cement grains have an average diameter of approximately  $10\mu\text{m}$  to  $20\mu\text{m}$ , and these set the scale for the microstructure.

Finally, the lower right image in Fig. 1 is a transmission electron micrograph of C-S-H

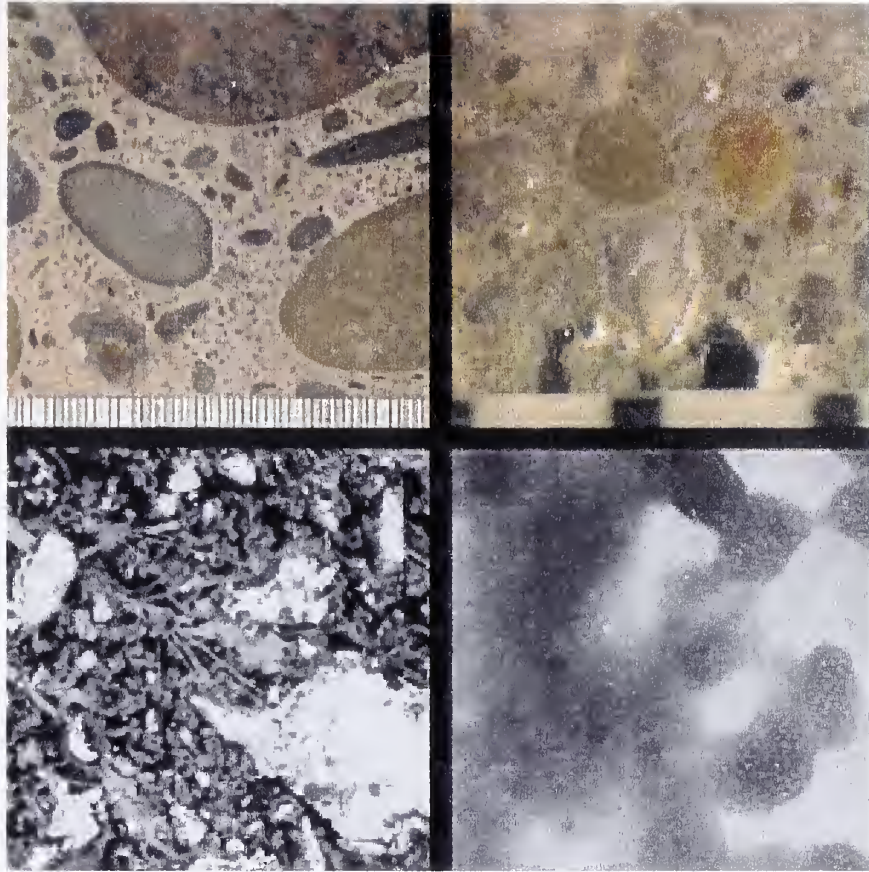


Figure 1: Showing concrete at four different length scales: upper left is concrete, upper right is mortar, lower left is cement paste, lower right is C-S-H.

[5], which is itself seen to be a complex material with a random porous nanostructure. The size of the image is about 300nm on a side. This random nanostructure can also be detected by neutron scattering [6].

The range of the random microstructure of concrete, from nanometers (C-S-H) to micrometers (cement paste) to millimeters (mortar and concrete) to meters (final end use) covers nine orders of magnitude in size! It is then a large and difficult task to try to theoretically relate the microstructure and the properties of concrete. This has led to the use of computer simulations, coupled with modern experimental probes, which have provided some insight into the microstructure.

## 2 Basic Concepts

Typical kinds of transport processes important in concrete are: 1) the transport of water, either due to a hydrostatic pressure head or wetting forces (capillary suction) and 2) the



migration of ions, either due to diffusion under a concentration gradient, or to transport by moving water. For both of these processes, how (and if) the relevant pores are connected to each other matters very much. Phrased more rigorously, the percolation properties of the random microstructure and particularly of the pore space are the critical geometrical and topological factors upon which the microstructure:transport property relationships are based.

The ideas of percolation theory are helpful in understanding the important features of random structures. The main concept of percolation theory is the idea of connectivity. Picture some sort of structure being built up inside a box by the random attachment of small pieces to each other. Percolation theory attempts to answer the question: at what point does the structure span the box? An alternate form of this question, for a random structure that already spans the box, is: if pieces of the structure are removed at random, when will it fall apart? The percolation threshold is defined by the value of some parameter, say volume fraction of the structure in the box, right at the point where the structure either achieves or loses continuity across the box.

An example of percolation phenomena is displayed by the model of randomly placing freely overlapping objects in a matrix (this actually roughly simulates the growth of solids due to reactions like those seen in concrete). The objects gradually form larger and larger clusters, because they can connect via overlap, until a percolated structure is formed. This model has been studied extensively in 2-D and 3-D (see Refs. [7] and [8] and many references therein). Consider the following simple 3-D example. The objects used are overlapping spheres, placed at random positions in a 3-D matrix. The volume fraction covered by the collection of spheres is monitored until they form a continuous structure. It is found numerically that they will become continuous when they occupy approximately 29% of the total volume [8]. This is an example of the percolation of a structure that is being randomly built up. If the spherical objects become ellipsoids, then this critical volume fraction decreases as the ellipsoid aspect ratio either increases or decreases away from unity [8]. For the sphere case again, if we now think of the matrix as a uniform conducting material, and the overlapping spheres as insulators, then the composite material will lose its ability to carry an electrical current when the matrix loses connectivity at a matrix volume fraction of about 3% [9]. This is an example of the percolation of a structure that is being randomly torn down. Concrete exhibits both kinds of percolation processes, at more than one length scale.

### 3 Cement Paste

We now specifically consider the microstructure-transport property relationships in cement-based materials. We begin with cement paste, as this is the matrix material for the concrete composite, and it is difficult to understand the behavior of a composite without first understanding the matrix phase. Later we will consider mortar and concrete, composites made from cement paste at higher length scales, and individual phases of cement paste like C-S-H, handled at lower length scales.

The starting point for cement paste = cement + water, cement powder, is obtained by grinding cement clinker. The cement clinker is manufactured by firing mixtures of limestone and clay, which contain aluminate and ferrite impurities. After extraction from the kiln,



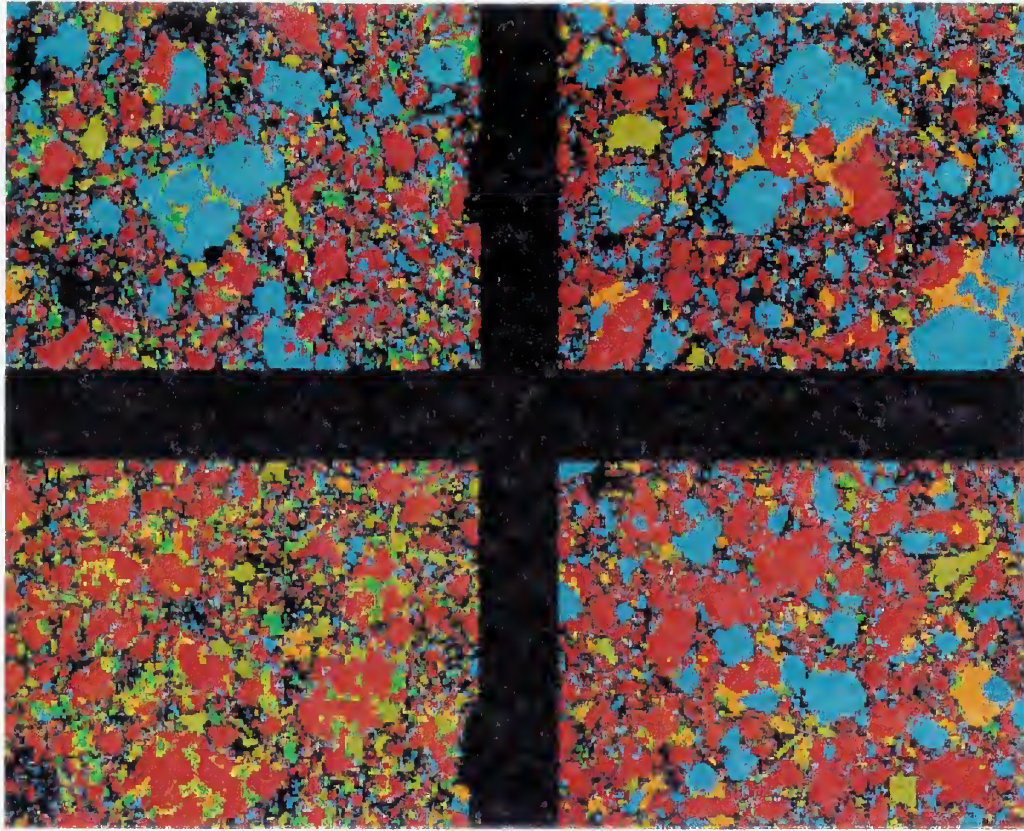


Figure 2: Showing processed and segmented SEM images of four kinds of portland cement particles. Each phase in the cement is identified by a unique color. The random microstructural differences between particles in the same cement, and between particles in different cements, is readily apparent.

gypsum (calcium sulphate dihydrate) is added to moderate the hydration process. After grinding together the clinker and gypsum, the cement powder consists of multi-size, multi-phase, irregularly shaped particles generally ranging in size from less than  $1\ \mu\text{m}$  to about  $100\ \mu\text{m}$ , with an average diameter of about  $15\ \mu\text{m}$  to  $20\ \mu\text{m}$ .

Figure 2 shows cross-sectional images of four different portland cements. These images were obtained by first taking a backscattered electron scanning electron micrograph, which determined the ranking of the average atomic number of each phase via the gray scale contrast. X-ray bitmapping was also carried out using the SEM in order to determine relative atomic abundance of important elements like calcium, silicon, aluminum, sulfur, and iron. By combining the x-ray and backscattered electron images, the principal chemical phases of the cement particles could then be determined [10]. Figure 2 clearly shows that even before hydration takes place, the cement powder is itself a random composite, with even most particles themselves being multi-phase composites.

When the cement is mixed with water, hydration reactions occur which ultimately convert



the water-cement suspension into a rigid porous material, which serves as the matrix phase for mortar and concrete. The nominal point of hydration at which this conversion to a solid framework occurs is called the set point. The degree of hydration at any time is the volume fraction of the cement that has reacted with water, and is often denoted by the symbol  $\alpha$ . The ratio of water to cement in a given mixture is specified by the water to cement ratio (w/c), which is the ratio of the mass of water used to the mass of cement used. An ordinary concrete used in buildings uses cement paste with  $w/c \approx 0.5$ . Newer high performance concretes often have w/c ratios of 0.3 or lower [11].

The various chemical and mineral phases within the cement powder hydrate at different rates, depending on their size and composition, and interact with one another to form various reaction products. Some products deposit on the remaining cement particle surfaces (surface products) while others form as crystals in the water-filled pore space between cement particles (pore products). For simplicity, and because it still correctly captures the main features of the pore structure, cement paste can be thought of as consisting of four phases: 1) unreacted cement, 2) surface products (like C-S-H), 3) pore products (like CH = calcium hydroxide), and 4) capillary pore space. Surface products grow outward from the unreacted cement particles and contain connected (percolated) gel pores, while pore products are generally polycrystalline and fully dense, with no connected pores. The capillary pores are the remaining water-filled space between solid phases, left over after a given degree of hydration takes place. Capillary pores generally range from about  $0.01\mu\text{m}$  to  $0.1\mu\text{m}$  in size, in a reasonably well-hydrated cement paste ( $\alpha > 0.5$ ), although in early hydration, they can range up to a few micrometers in size.

While images of both initial and hydrated cement microstructures can be experimentally obtained in two dimensions, acquiring quantitative three-dimensional information is much more difficult. It is for this reason that computer models of the 3-D microstructural development of cement paste have been developed.

The actual process of cement hydration, for the purposes of modelling the development of microstructure, can be broken down into three parts: 1) material dissolves from the original cement particle surfaces, 2) diffuses within the available pore space, and 3) ultimately reacts with water and other dissolved or solid species to form hydration products. Therefore, in order to simulate the microstructure development of hydrating cement, the physical processes of dissolution, diffusion, and reaction must be simulated. Each of these processes may be conveniently simulated using cellular automaton-type rules as has been previously described [12, 13]. Figure 3 shows four steps of simulated hydration for a  $C_3S$  cement paste in 2-D. The original particle shapes are taken from a backscattered SEM image. The images have been colorized according to the major phases of portland cement [12].

This brief description of the chemical hydration process, which is the basis of the microstructural formation of cement paste, of course glosses over a number of chemical details, many of which are not clearly understood [12]. However, this simple description is sufficient to be able to go on and investigate the various important percolation thresholds that occur in cement paste.



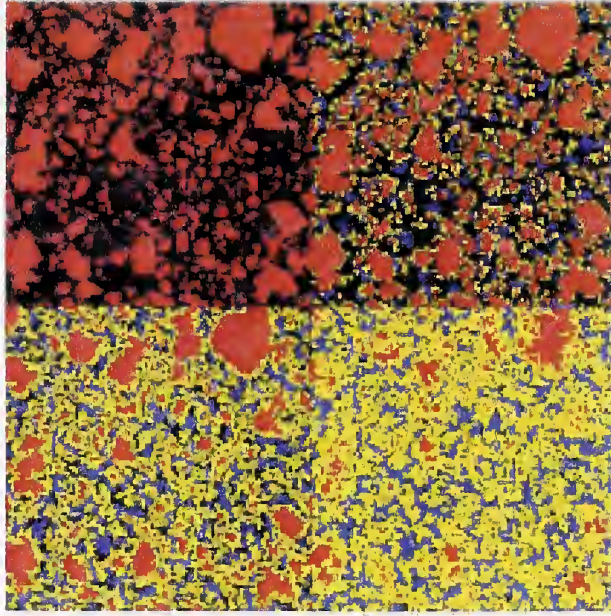


Figure 3: Showing four stages of hydration in a microstructural model of  $C_3S$  hydration. The degrees of hydration are: top left–0, top right–20 %, bottom left–50%, bottom right–87%. Red=unreacted cement, blue=CH, yellow=C-S-H, and black= porosity.

### 3.1 Solids percolation: set point

Immediately after mixing cement powder and water together, the solid phases are discontinuous, or connected only via van der Waals-type forces [14], and so the freshly mixed cement paste is a viscous liquid. The solid phase is then built up through random growth of reaction products, and at some point becomes continuous across the sample, mainly due to the formation of the C-S-H surface products [15]. Experimentally, this setting process can be detected using a needle penetration test [16], ultrasonic shear wave propagation [17], or by measuring the shear strength of the paste [14, 18]. The set point can be defined rigorously, using percolation concepts, as the point where percolation of the total solid phase occurs. This point can be computed, using a three-dimensional computer model based on a simplified cement composed only of monophase  $C_3S$  particles. This chemical simplification of the particles is justified by the experimental observation that the C-S-H surface product causes set [15] and by the fact that this simple model generates almost the same quantity of surface products as those produced in real cements [19]. Also, most real portland cements are usually composed of at least 60%  $C_3S$ .

Using this model, in conjunction with a burning algorithm [19] to compute connectivity, one can determine the degree of hydration necessary to first have a continuous network of cement particles linked by C-S-H gel product. This seems to be a reasonable definition of set, especially since the combined phase of cement and C-S-H will percolate before any



individual solid phase. In addition, the original configuration of the cement particles can be simulated as being flocculated or dispersed. Figure 4 shows a quantitative comparison between model and experimental results.

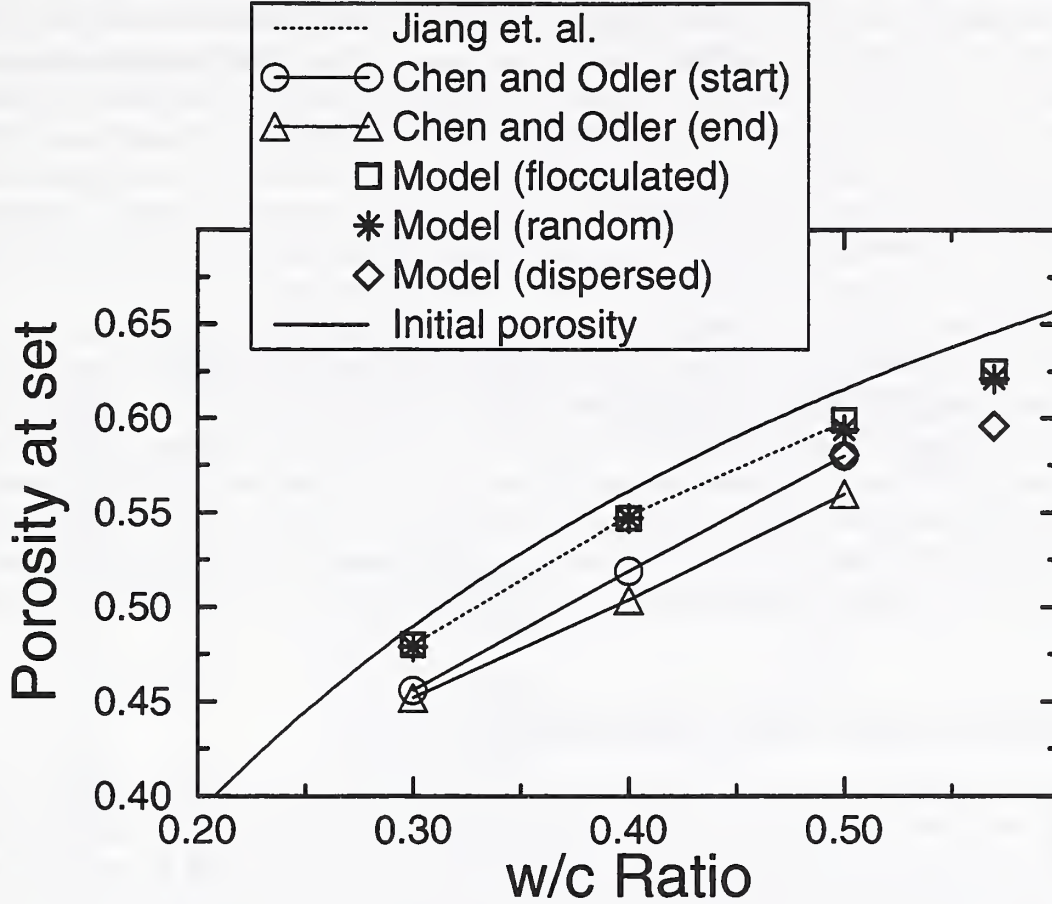


Figure 4: Showing the capillary porosity remaining at the set point, for several experimental and model cement pastes involving different initial cement particle configurations, as a function of the w/c ratio of the cement paste.

The data from Jiang et al. [18] were calculated as the capillary porosity at the point where the cement paste exhibited a shear resistance of 0.08 MPa. The data points of Chen and Odler [15] correspond to the measured porosities at the beginning and end of set according to the ASTM standard needle penetration method [16]. Model results, corresponding to the point when a spanning cluster of  $C_3S$  particles connected together by the C-S-H gel first exists, are presented for flocculated, random, and dispersed systems based on a discretized version of a real measured particle size distribution [20, 21]. In general, the comparison among these three data sets is reasonably good, particularly so for the experimental data of Jiang et al. [18] and the model results for the random/flocculated systems. As the w/c

ratio decreases, less hydration is needed to achieve set, since the initial interparticle spacing is less. Based on the model results for random systems, degrees of hydration of 1.8%, 2.7%, and 4.6% are required to achieve solids percolation for w/c ratios of 0.3, 0.4, and 0.5. The capillary porosities at set obtained by Jiang et al. [18] are consistently higher than those of Chen and Odler [15], suggesting that the ASTM needle penetration test method measures set time based on a resistance somewhat greater than that corresponding to a shear strength of 0.08 MPa. As might be expected, in general, the model flocculated systems require less hydration to achieve set than their dispersed counterparts, in agreement with experimental studies [22, 23]. It should be noted that the experimental measurements were generally made on portland cements while the model results are for  $C_3S$  pastes. However, the similarity in volumes of surface and pore products formed for these two pastes [19] allows valid comparisons to be made between model and experimental results.

Because it is the connection of cement grains by C-S-H gel product that regulates set, a finer particle size cement will actually require a greater degree of hydration to achieve set than a coarser one. Thus, even though a finer cement typically hydrates at a faster rate, it may lead to a longer setting time than a coarser, slower hydrating cement, where fewer particle-to-particle contacts are necessary to achieve set, as has been verified experimentally [14]. This analysis assumes that the volume of C-S-H product needed to connect two cement particles is roughly invariant, so that as the particle size increases at a fixed total volume of cement, the number of particles and therefore the number of connections needed will decrease [24].

### 3.2 Capillary pore space percolation

A percolation threshold that is more important for transport processes is the point at which the capillary pore space no longer percolates. Such a percolation threshold can exist, because as hydration products are formed, pieces of the capillary pore space will be trapped and cut off from the main pore network, thus reducing the fraction of the pores that form a connected pathway for transport. As this process continues, the capillary pore space can lose all long-range connectivity, so that fast transport of water or ions through the relatively large capillary pore system would end, and slow transport would then be regulated by the smaller C-S-H gel pores (pore product).

Computer simulation of cement hydration in 3-D is a means of computing such a percolation threshold. Fig. 5 shows the Fraction Connected of the capillary pore space vs. degree of hydration for several w/c ratios, as computed by a computer simulation model of cement paste microstructure [19]. The quantity Fraction Connected is defined as the volume fraction of capillary pores that make up a connected path through the sample, divided by the total volume fraction of capillary pores.

Immediately after mixing, the cement particles are totally isolated, assuming adequate dispersion, and so the connected fraction of the capillary pore space is one. As hydration occurs the connected fraction decreases gradually. If continuity is lost at some critical degree of hydration, the Fraction Connected will go to zero. Such a percolation threshold can be seen in all of the w/c ratio results plotted, except for 0.6 and 0.7. We have found in the model that w/c ratios of 0.6 and above always have a continuous (or percolated) capillary pore system. This prediction is in good agreement with experiment [25]. It is clearly seen in

Fig. 5 that as the w/c ratio decreases below 0.6, less and less hydration is required to close off the capillary pore system.

In order to unify the previous results, we have re-plotted all the data from Fig. 5 in Fig. 6 against capillary porosity. All the connectivity data now falls on one curve, and it is clearly seen that there is a common percolation threshold at a critical value of capillary porosity of about 0.18.

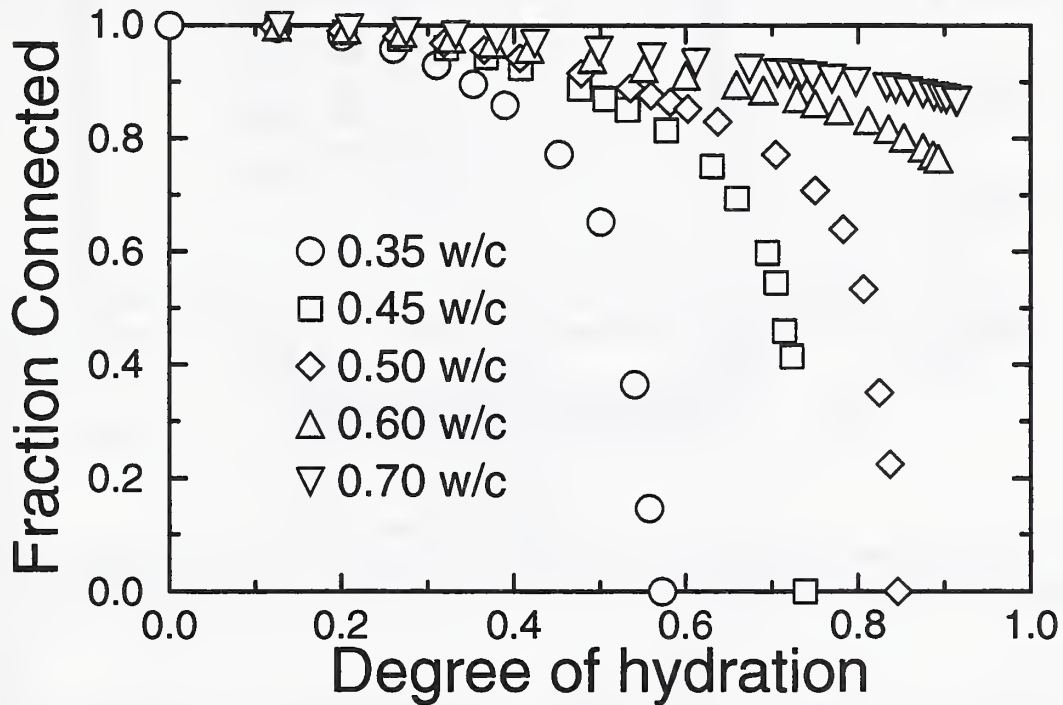


Figure 5: Showing the fraction of the capillary pore space that is part of a percolated (continuous) cluster, for several different w/c cement pastes as a function of degree of hydration.

Even the 0.6 and 0.7 w/c data fall on this curve, and now it is clear why these pastes always have an open capillary pore space: there is not enough cement present originally to be able to bring the capillary porosity down to the critical value, even after full hydration. The capillary pore space percolation threshold for cement paste will have some sensitivity to cement particle size distribution and degree of dispersion, so that the critical value of capillary porosity for percolation should be considered to be about  $18 \pm 5\%$ . This range of values is a rough estimate of finite system size and particle size distribution effects, based on computation on different systems.

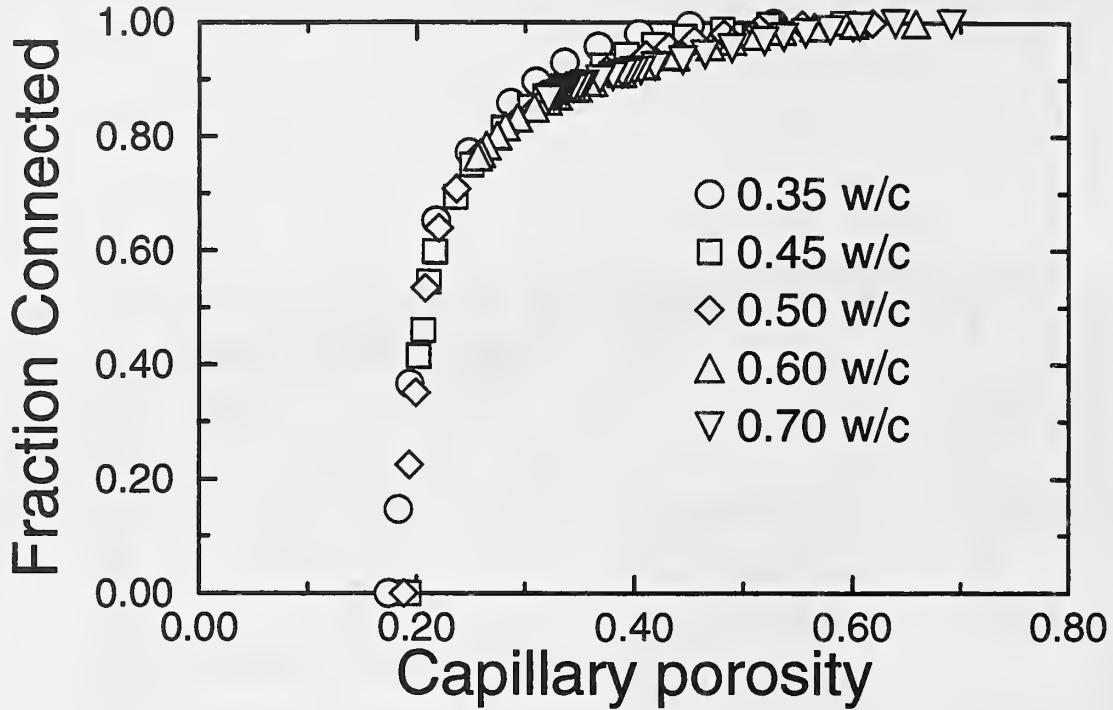


Figure 6: Showing the fraction of the capillary pore space that is part of a percolated (continuous) cluster, for several different w/c cement pastes as a function of capillary porosity.

The percolation threshold is also sensitive to the morphology of the reaction products, reminiscent of the simple overlapping object percolation problem [8]. For example, in a simple dissolution/reaction model, in which only a pore product is formed, capillary porosity percolation thresholds have been computed that are on the order of 20% for totally random morphology products, 25% for 1-D needle-like products, and 30% for plate-like products [26].

### 3.3 C-S-H percolation

As was discussed above, the percolation of the combined cement:C-S-H phase is what determines the set point, or the rigidity threshold. The model described above also, however, predicts a percolation threshold for the C-S-H phase by itself. The prediction is that the C-S-H phase, independent of w/c, will percolate when its volume fraction is about 20% [19]. This will be fairly early in the hydration process, but well after the set point. Since this percolation threshold is not usually connected to a physical observable at this stage, it is difficult to experimentally validate this prediction. Recently, however, electrical measurements

at low temperature ( $-40^{\circ}$ ) have been able to confirm this prediction. Both the capillary pores and the C-S-H pores serve as conducting channels, since they are filled with the electrolytic pore solution [27]. At lower temperatures, the water in the larger capillary pores freezes while that in the smaller C-S-H pores does not. In this case, the electrical conductivity of the capillary pores is turned off, and the only conductivity comes from the C-S-H pores. If the C-S-H phase is not percolated, then the conductivity should be very small. Figure 7 shows the conductivity at a temperature of  $-40^{\circ}$ , normalized by the pure C-S-H conductivity and plotted vs. volume fraction of C-S-H. There is a clear percolation threshold at around 20% volume fraction, validating the predictions of the model [28]. There is also excellent agreement between model and experimental values for all the volume fractions of C-S-H examined. The simple fact that the conductivity goes *up* with hydration shows that at this temperature, the conductivity is coupled to the growing C-S-H phase, not the shrinking capillary porosity phase.

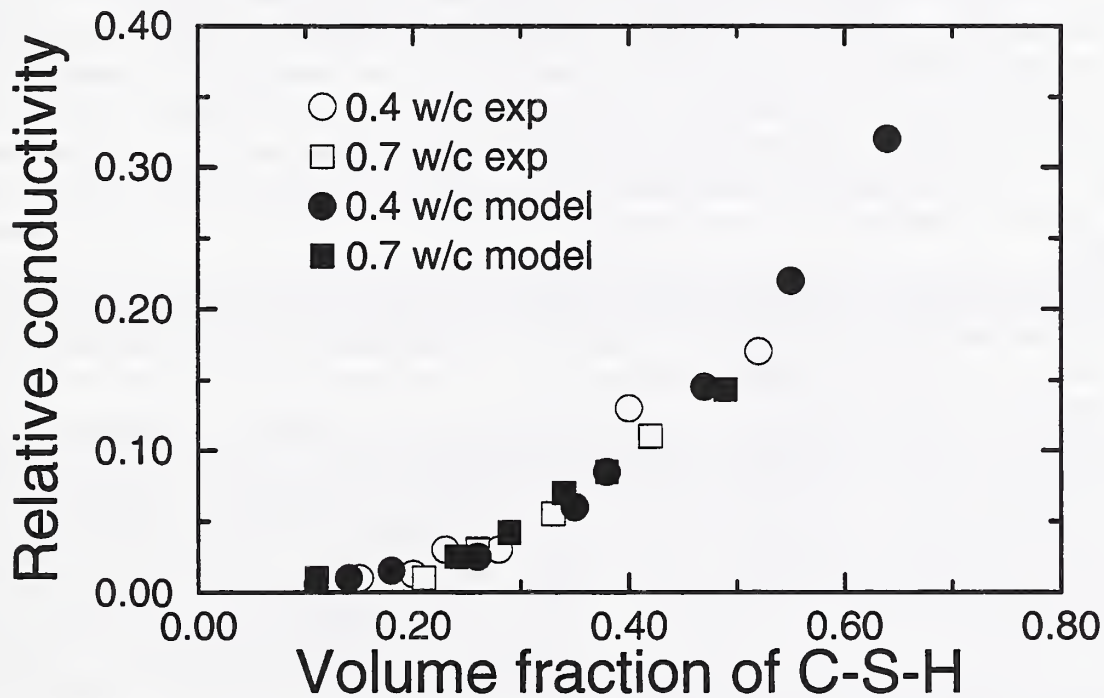


Figure 7: Showing the electrical conductivity of the cement paste at  $-40^{\circ}$ , plotted vs. the volume fraction of C-S-H. The solid symbols are model results, and the open symbols represent experimental values.

### 3.4 Cement paste pore size

During hydration, the capillary pore size, as well as the overall capillary porosity, decreases due to consumption of water during hydration, producing hydration products that fill in the capillary pore space. The size of the gel pores are fixed by the structure of the C-S-H, however, and so remain relatively constant in size. As hydration continues, the size of the smallest capillary pores decreases to roughly the 10 nm gel pore size [2, 29]. Therefore the importance of the pure capillary pore transport paths decrease with time due to decreasing capillary pore size as well as decreasing pore connectivity.

### 3.5 Diffusivity of Cement Paste

Building on the percolation and pore size results given above, the dependence of the diffusivity of cement paste on pore structure can now be qualitatively outlined. Early in the hydration process the capillary pore space is fully percolated. These pores are much larger than the C-S-H gel pores (which are themselves also fully connected fairly early in the hydration process [19]) and so dominate the transport. As the capillary porosity decreases, the capillary pores become smaller and only partially connected, so for porosities near but above the percolation threshold, pure capillary pore paths have only slightly more influence on flow than the hybrid paths that are made up of isolated capillary pockets linked by C-S-H gel pores. The capillary pores are still somewhat bigger than the gel pores, but their connectivity is decreasing. Below the critical capillary porosity, all flow must now go through C-S-H gel pores, but flow will be dominated by paths that still contain some isolated capillary pore regions, and are not just made up of pure C-S-H gel pores. If this were not true, then after a certain point, the diffusivity would begin going up with increasing hydration, since more C-S-H, and thus more gel pores, were being formed. This has not been observed in cement paste [30].

The same microstructure model used to predict the connectivity results shown in Figs. 5 and 6 can also be used to compute the diffusivity of cement paste by solving Laplace's equation in the pore space with a finite difference method [30]. Because of the Nernst-Einstein relation [30, 31], relating diffusivity and conductivity, the same mathematical apparatus can be used for both, so that solutions to the time-independent Laplace's equation apply equally well to diffusivity or conductivity. If  $D_o$  is the ionic diffusivity in free water,  $\sigma_o$  is the conductivity of the electrolytic pore solution,  $D$  is the measured diffusivity of the porous material, and  $\sigma$  is the measured conductivity of the porous material, then the physical content of the Nernst-Einstein relation is that  $D/D_o = \sigma/\sigma_o$ . This computational procedure can be done for the DC and also for the frequency-dependent AC conductivity [32, 33]. Computational results confirm the above microstructural picture, and compare reasonably well to experimental measurements [30, 32, 33, 34].

Figure 8 shows comparisons between experiment and model results for an 0.5 w/c cement paste [34]. The quantity  $\Gamma = \sigma/\sigma_o$  is called the relative conductivity or diffusivity [30, 34]. The value of  $\sigma_o$  was found by first squeezing out the electrolytic pore solution in a high-pressure press, and then measuring the conductivity of the pore solution in an impedance spectrometer [34]. A reasonably good comparison exists between simulation and experiment over a wide range of capillary porosity, indicating that the capillary pore space of the model

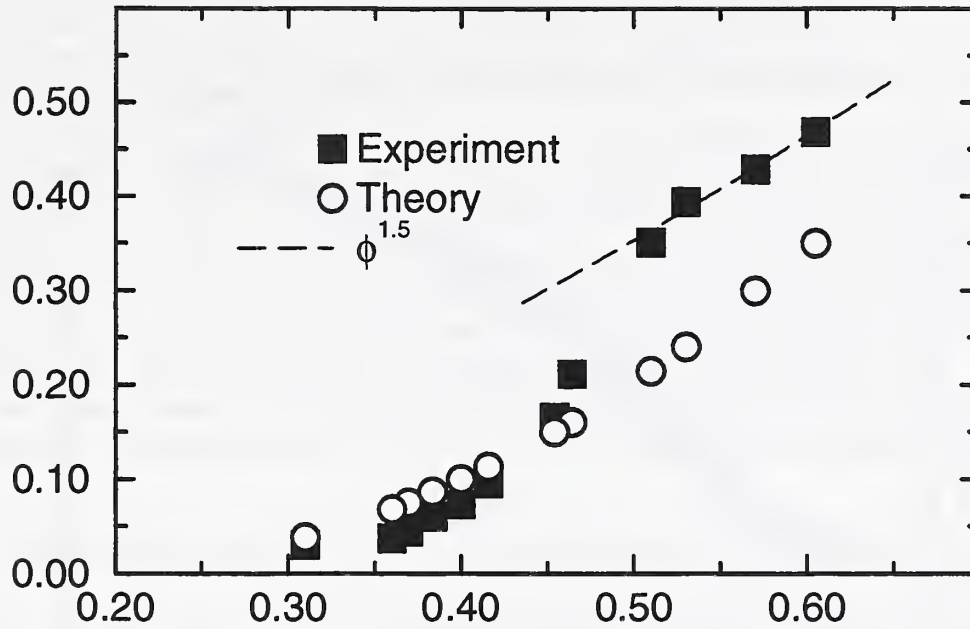


Figure 8: Showing cement paste conductivity results, normalized by the pore fluid conductivity, for an 0.5 w/c cement paste as a function of the capillary porosity.

compares well to that of real cement paste. The model results are from an equation that was fit to the results shown in Fig. 9 [30]. They were determined from fairly low porosities, and so are not expected to fit well at high porosities. The agreement across all porosities is within a factor of two, however. The  $\phi^{1.5}$  power line shown is the result for suspensions of insulating, reasonably spherical objects suspended in a conducting medium. When hydration begins, ions are released into the mixing water, turning it conductive, while the cement simply acts as suspended insulating particles, which grow in size with hydration and so increase in volume fraction  $1 - \phi$ . However, as can be seen in the figure, the hydrating cement paste quickly changes its topology as the solid phase connects (set point), and the measured conductivities drop below the  $\phi^{1.5}$  curve.

Figure 9 shows a collection of model results for  $\Gamma$  for different w/c values, all plotted against capillary porosity. Notice how all the data falls on a single master curve, as did the capillary pore space percolation data, when plotted against capillary porosity [30].

Such a qualitative result has been observed experimentally as well [35], lending support to the basic correctness of the model and the percolation picture of cement paste pore structure.

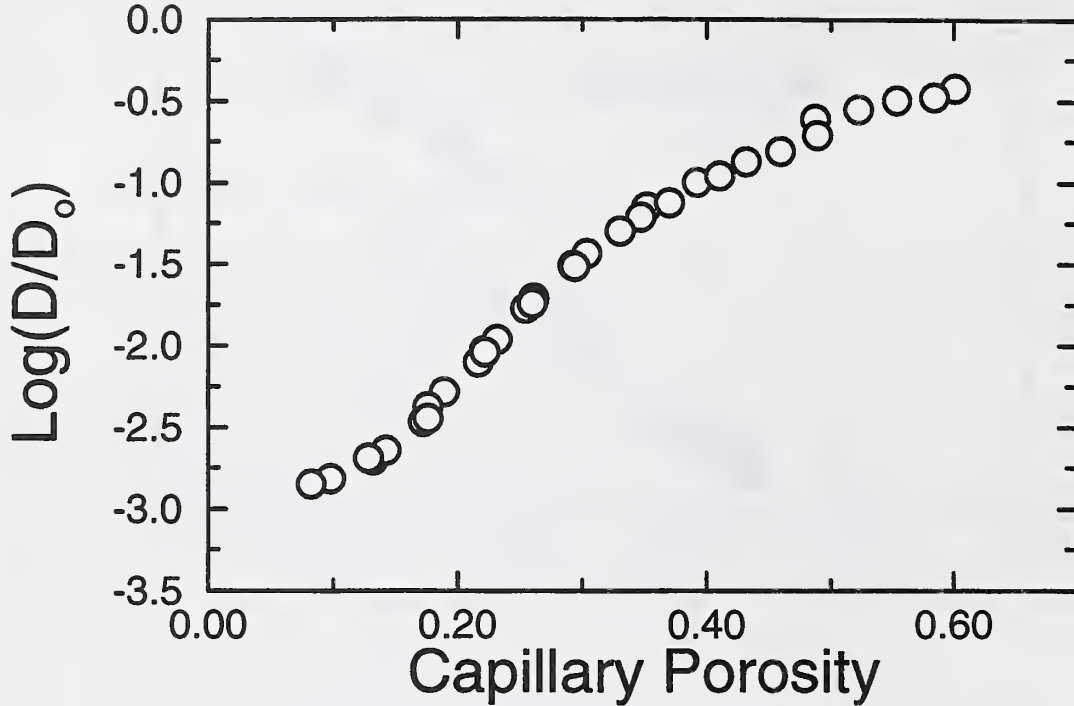


Figure 9: Showing model data for the diffusivity for several different w/c cement pastes, normalized by the free water diffusivity, all plotted vs. capillary porosity.

A recent review (and references therein) may be referred to for more details of the electrical conductivity/ionic diffusivity of cement paste [36].

### 3.6 CH percolation: Leaching

We can now combine the percolation and diffusivity simulations and ideas to study the problem of CH (pore product) leaching in cement paste. As concrete is exposed to the elements, its underlying microstructure can be attacked by a variety of aggressive agents. For example, rainwater and groundwater can degrade the concrete by dissolving soluble constituents such as calcium hydroxide. Using computer simulation, we can study the effects of calcium hydroxide dissolution on: 1) the percolation properties of the capillary pore space, and 2) the relative ionic diffusivity.

The microstructure model shown in Fig. 3 for  $C_3S$  cement paste was used to produce a hydrated specimen which was subsequently subjected to the leaching process in which CH was randomly removed. This specimen can start with either a percolated or a disconnected

capillary pore space. From a percolation perspective, the key point is the connectivity of the combined capillary porosity and calcium hydroxide phases. If these two phases together form a connected pathway across the microstructure, the capillary porosity will certainly be percolated when the calcium hydroxide is leached away, regardless of its initial percolation state. Based on computer simulation, a volume fraction of 16-20% for the combined capillary porosity and leachable calcium hydroxide phase is sufficient to form a percolated pathway after leaching has taken place [37].

The computer models have also been applied to computing the increase in diffusion coefficients due to the leaching of calcium hydroxide from fully hydrated  $C_3S$  pastes of various w/c ratios [37]. The removal of all the CH from a cement paste can result in a multiplicative increase in diffusivity of up to about 50 times that of the original paste, as computed from the model, if the unleached paste had a disconnected capillary pore space and leaching re-connected it. In Figure 10, model values are compared with experimental results [36] in which the diffusion coefficients of cesium and tritium were measured as a function of the amount of CH leached out of portland cement paste specimens. Reasonable agreement is exhibited between the model and the available experimental results.

## 4 Microstructure of Mortar and Concrete

Mortar and concrete are random composite materials, with the fine and coarse aggregate acting as the inclusions and the cement paste acting as the matrix. The only real difference between mortar and concrete is in the size of the aggregates used. Typically, the maximum aggregate diameter in a mortar is 1mm to 3 mm, while the maximum aggregate diameter in a commercial concrete is around 30mm. Concrete used for dams and other such structures, known as mass concrete, can have aggregate diameters even up to 150mm or so [39].

To handle mortar and concrete theoretically, we average out the cement paste micrometer length scale to avoid having to deal with microstructure on too wide a range of length scales at the same time. The transport properties of the aggregate are measurable and usually constant in time, while the transport properties of the cement paste depend on the original water:cement ratio, kind and quantity of admixtures, hydration time, and to some degree on the initial particle size distribution. However, it will be shown below that the interfacial transition zone between the cement paste and aggregates may play a critical role in determining the bulk transport properties [40]. Therefore, when averaging over the cement paste microstructure, the micrometer scale interfacial transition zone, which is determined from cement paste microstructure, must not be omitted. This makes the concrete random composite problem difficult, since micrometer and millimeter length scales have to be simultaneously considered. Also, mortar and concrete have aggregate volume fractions of up to 70% or so, which implies that the spacing between particle surfaces is on the order of  $100\mu m$ , as seen by SEM in cross-section [41]. Therefore the micrometer cement paste scale can also clearly come in here, especially, as we will see below, as the interfacial zone is itself on the order of  $20\mu m$  to  $50\mu m$ . There has also been some work using x-ray microtomography to directly image the aggregate-matrix structure in mortars, and in particular the spacing between aggregate surfaces, in three dimensions [42].

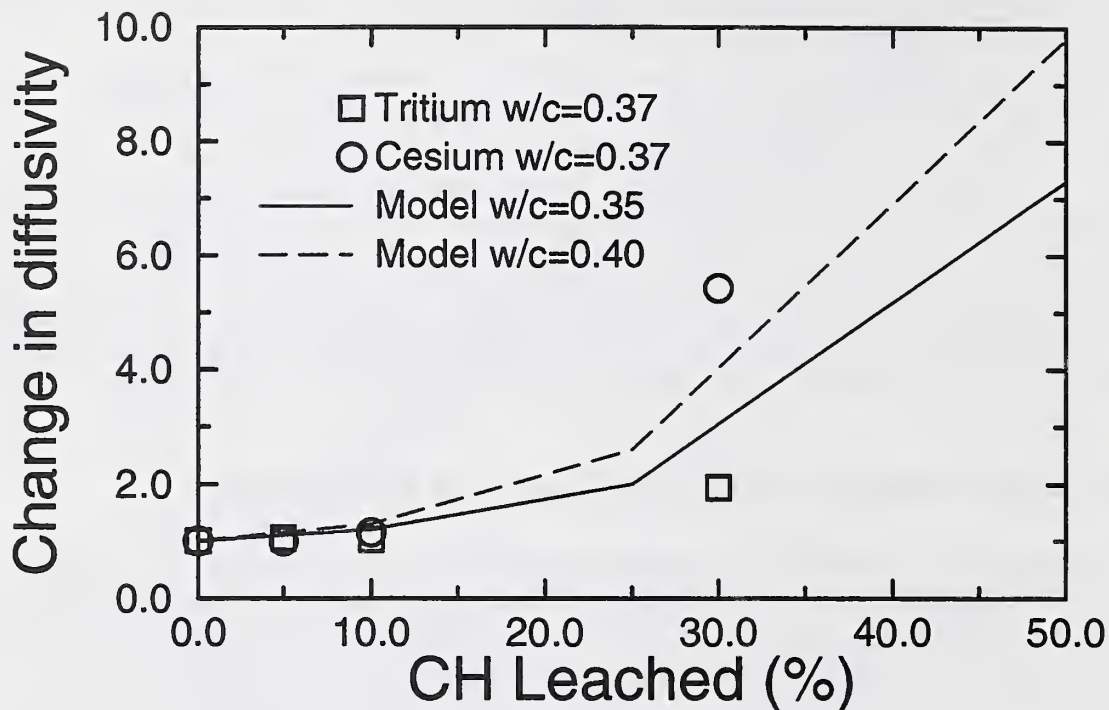


Figure 10: Showing experimental and model results for how the relative diffusivity changes as the amount of CH leached away increases.

#### 4.1 Interfacial Zone Microstructure

Characteristic features of the interfacial transition zone, that region of the cement paste close to an aggregate surface, are higher capillary porosity and larger pores than in the bulk cement paste matrix [43, 44]. These features are typically seen in the cement paste that is within  $50\mu m$  of an aggregate surface [45]. Using the cement paste microstructure model mentioned above, we have analyzed two major causes of these features in the interfacial transition zone microstructure: 1) the particle packing effect, and 2) the one-sided growth effect [46].

The particle packing effect arises from particles not packing together as well near a flat surface as in free space. Since the typical aggregate is many times larger than the typical cement particle, even for the fine aggregate, locally the aggregate surface appears flat to the surrounding cement particles. This inefficient packing causes less cement and higher porosity to be present initially near the aggregate surface, and so even after hydration this condition persists. The width of the interfacial transition zone will then scale with the

median cement particle size [47]. This is the main contribution to the interfacial transition zone microstructure, but not the only one.

The one-sided growth effect arises in the following way. Consider a small region of capillary pore space located out in the bulk paste part of a mortar or concrete. On the average, there is reactive growth coming into this small region from all directions, since the cement particles are originally located randomly and isotropically. Now consider a similar small region of capillary pore space, but located very near an aggregate surface. Reactive growth is coming into this region from the cement side, but not from the aggregate side [46]. This will give rise to a higher porosity, as the net growth of solids will then be smaller in the interfacial transition zone region.

## 4.2 Concrete considered as a composite material

If we were to make a concrete using cement paste and zero porosity aggregate, with no interfacial transition zones present, the ionic diffusivity and fluid permeability of the concrete would rigorously have to be lower than the corresponding values for the cement paste, as predicted by analytical bounds like the Hashin bounds [49]. This is because the aggregates, assumed to be fully dense, would have transport coefficients of zero, so that the mixture must have lower bulk properties, which can only decrease as more of the second phase (aggregate) is added. However, having a third phase, the interfacial transition zones, can modify this picture.

The study of the transport properties of concrete using composite theory then requires, as experimental input, simultaneous measurement of the cement paste host and concrete transport properties while the aggregate volume fraction is systematically varied. Unfortunately, there are not many experimental results available [50, 51]. Results from recent work, however, demonstrate that the effective transport properties of concrete can increase greatly as more aggregate is added past a critical amount [52]. There are also data showing that concrete can have up to 100 times the water permeability of the cement paste from which it is made [2]. Experimental results for the ionic diffusivity show effects beyond that of simply adding insulating, non-porous aggregate to a porous phase [50, 51]. Elastic modulus data also clearly show the effect of a third phase, the interfacial transition zone phase [53, 54, 55]. The only possible microstructural explanation of all this behavior, besides that of an unreasonable amount of microcracking, is the effect of transport of fluid or ions through the interfacial transition zones. It is already known that the interfacial transition zone regions contain pores larger than those in the bulk paste. However, if the interfacial transition zones do not percolate, their effect on transport will be fairly small, as any transport path through the concrete would have to go through the bulk cement paste. Transport properties would then be dominated by the bulk cement paste transport properties.

Before exploring the interfacial transition zone percolation problem further, it is important to note that real concrete always contains air voids, especially in air-entrained concrete, where air voids are introduced deliberately to help the porous material resist freeze-thaw damage [56, 57]. The volume fraction of air voids can be as great as 5-10%, so they are an important constituent of concrete [56, 57]. As long as they remain filled with air, they can be treated in a transport model simply as more zero-property aggregate, with a known size distribution [56, 57], since the presence of air voids also causes interfacial transition zone

regions to develop [58].

### 4.3 Interfacial Zone Percolation

Effects of the percolation of the interfacial transition zones can be observed from mercury porosimetry data [59]. Cement paste by itself has a certain threshold pore diameter, corresponding to a certain mercury pressure. For mercury pressures below this value, the mercury only intrudes the surface of the sample. For mercury pressures above this value, the mercury percolates throughout the material. When aggregate is added, this threshold diameter does not increase at first, but remains at a value typical of cement paste. As the volume of aggregate increases to a critical value, the mercury breakthrough pressure or critical diameter abruptly changes from values typical of bulk cement paste to those typical of the interfacial transition region, pore sizes roughly ten times bigger. This is interpreted as the point at which there are enough aggregates present so that the associated interfacial zones can overlap and percolate [59].

To study the percolation or connectivity of the interfacial transition zones in concrete is computationally not simple, as the geometry of this phase is complex. Fortunately, in the percolation literature there is a model that is perfectly suited for this study, the hard core/soft shell (HC-SS) model [60]. This model starts with a random suspension of hard spherical particles, which are hard in the sense that they are packed without being allowed to overlap, as in a suspension. Then concentric spherical shells are placed around each particle, where the spherical shells all have the same thickness, and are allowed to freely overlap. The volume fraction of shells required to make the shells percolate, which is when a continuous soft shell pathway first becomes established, is then computed. The volume fraction of soft shells required for percolation is a function of how many hard core particles are present, and the thickness of the soft shell. Obviously, when more hard core particles are packed in a given volume, there is less space between them, so that thinner soft shells will be sufficient for percolation. When there are fewer hard core particles present, thicker shells will be required for percolation of the shell phase. For concrete, clearly the hard cores correspond to the aggregates, and the soft shells to the interfacial transition zones. In the percolation literature, usually the value of  $h$  varies for different radii ( $r_i$ ) particles, such that the ratio  $(r_i + h)/r_i$  remains constant for different radii  $r_i$ . In the case of concrete, the value of  $h$  remains constant for different particle radii, which implies that this ratio is different for different radius particles.

Figure 11 shows a two dimensional slice through a simple HC-SS three-dimensional model of a mortar, where four different sizes of spherical sand grains were used, ranging between 0.5 and 3 millimeters in diameter [61]. Note that there are more than four diameters of particles apparently present in the picture, because the slice did not always go through sphere centers. In this two-dimensional slice, the interfacial zone regions do not appear to percolate at all. As a further example, Fig. 12 shows slices through two other similar systems, but with both having a wider range of aggregate sizes than in Fig. 11. The right hand system in Fig. 12 is built up of ellipsoidal particle shapes [62].

To study the percolation in 3-D of the interfacial transition zones, it is good to first consider a simple, yet non-trivial example of these ideas: a HC-SS model for monosize spherical hard spheres [63, 64]. We study the percolation of the soft shell for different

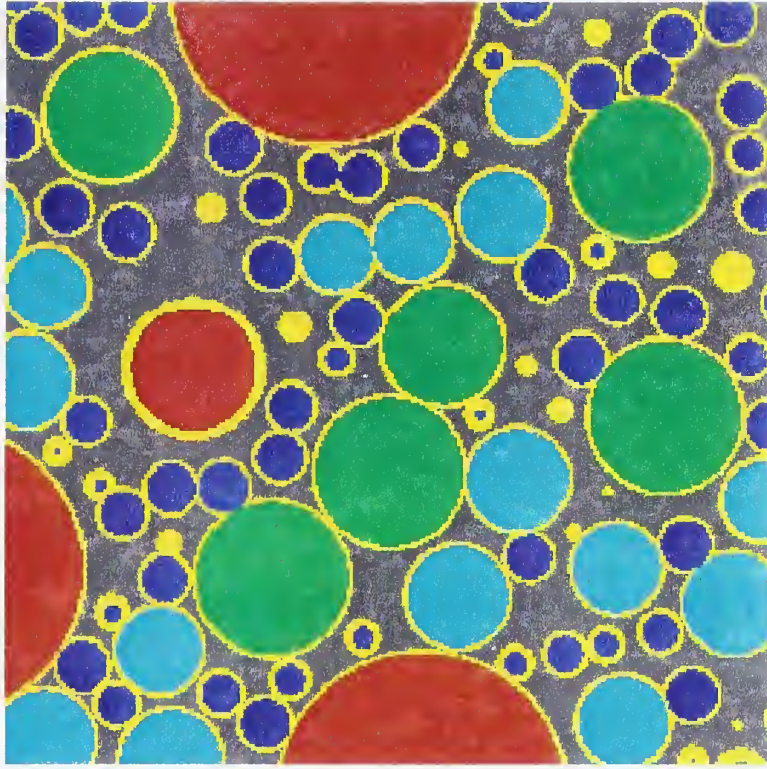


Figure 11: Showing a slice of a three dimensional model of mortar, with four aggregate diameters ranging between 0.5mm and 3mm. The four colors (dark blue, light blue, green, and red, indicate, from small to large, the four aggregate sizes used. The interfacial transition zone is shown as yellow.

thicknesses of the shell ( $h=a-b$ ) compared to the radius of the hard cores ( $b$ ). The total radius of the composite particle is  $a=b+h$ . The relevant variable in this case is the ratio  $b/a$ , where  $b/a = 0$  is just the overlapping sphere problem mentioned earlier in the chapter, and  $b/a = 1$  is the random sequential absorption or random parking problem for non-overlapping spheres in 3-D [65]. The larger the value of  $b/a$  (i.e. the thinner the shells), the greater the value of the volume fraction of hard cores,  $c$ , that will be required and the smaller the fraction of space that will be occupied by the percolating shells. Figure 13 shows the volume fraction of the shells at percolation vs.  $b/a$ .

At  $b/a = 0$ , we get a volume fraction of 0.29 [8], and as  $b/a \rightarrow 1$ , the volume fraction of the shells needed to percolate goes to zero [66]. Shown also are the value of the limiting concentration  $c \approx 0.38$  for mono-size random parking [65], and curves based on an effective medium theory [66]. Note that there is a threshold value of  $b/a \approx 0.9615$  above which it does not seem possible to form connected percolating shells based on the random parking algorithm for monosize spheres.

To study interfacial transition zone percolation in concrete, we take a fixed shell thickness to represent the interfacial transition zone, and then randomly place spherical aggregate



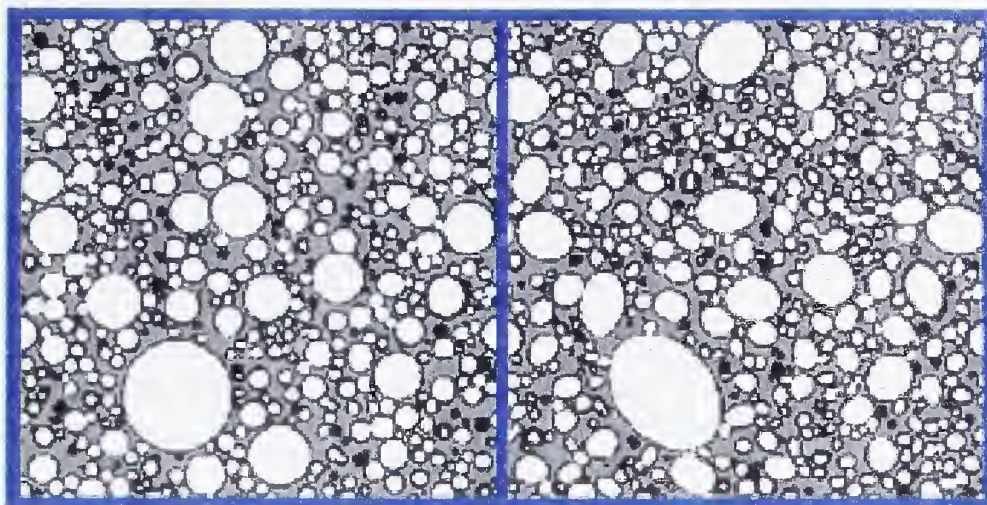


Figure 12: Showing slices of two different three dimensional concrete models, with spherical and ellipsoidal shaped aggregate particles. Aggregates are white, bulk cement paste is gray, and the interfacial transition zones are black.

particles that are then each surrounded by these shells. The width of the interfacial transition zone should be independent of aggregate size, as long as the median aggregate size is at least 5-10 times the median cement particle size, and will depend only on the median cement particle size [47]. The size distribution of the hard core particles are taken from measured aggregate size distributions [59, 67, 68, 69]. The fraction of the total shell volume that forms part of a connected cluster is then computed as a function of the volume fraction of aggregate present.

Results for a mortar [59, 68, 69] are shown in Fig. 14, in which each curve shows the connectivity of the interfacial transition zones for different choices of interfacial transition zone thickness.

When comparing against portland cement mortar mercury intrusion data [59, 68, 69], it was found that a choice of  $20\mu\text{m}$  for the interfacial transition zone thickness gave the best agreement with the mercury data. The mercury data gave an idea of what the percolation threshold of the interfacial transition zones was by showing a large increase in large pores intruded at the mercury breakthrough point [70] at a certain aggregate volume fraction. The width given in scanning electron microscopy studies of the interfacial transition zone,  $30\text{--}50\mu\text{m}$ , is defined by measuring from the aggregate edge to where the measured porosity assumes its bulk value. This would not be the width seen by mercury porosimetry, because it is probable that the larger pores will be found in the larger porosity regions nearer to the aggregate, which will be seen first by the mercury. Also, as to the effect on transport properties, the inner region of the interfacial transition zone is of more importance, since its transport properties will be higher than the outer region because of the larger pore size and porosity. The width of  $20\mu\text{m}$  given by the hard core/soft shell model is then an effective width, where this width contains the larger pores that would be important for transport.



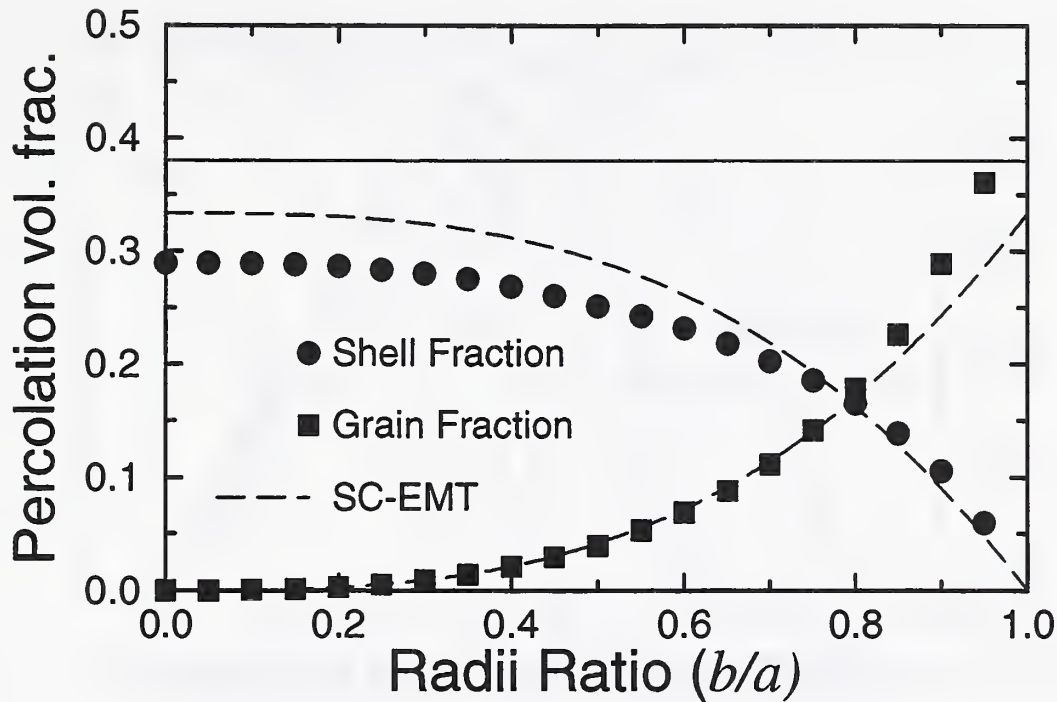


Figure 13: Showing the volume fractions of the hard cores and the soft shells when the soft shell phase has just percolated, for monosize spherical hard core particless. The solid lines are from an effective medium theory described later in the text.

Figure 14 also shows that for an aggregate volume fraction of 40% or more and an interfacial transition zone thickness of at least  $20\mu\text{m}$ , the interfacial transition zones will be percolated at least partially, and will be fully percolated for aggregate volume fractions greater than 50%. Most concretes have aggregate volume fractions well above 50%, so that in general, we can conclude that the interfacial transition zones in usual portland cement concrete are percolated, and so will have an effect on transport properties.

The fraction of the cement paste that lies in interfacial transition zones can also be calculated using the hard core/soft shell model for a given aggregate volume fraction and particle size distribution. Results are given in Fig. 15 for a specific mortar and concrete [59]. Figure 15 shows that, for the mortar, quite a large part of the cement paste matrix lies within an interfacial transition zone, with about 20% lying within  $20\mu\text{m}$ , and about 50% lying within  $50\mu\text{m}$  of an aggregate surface. For the concrete, the volume of cement paste matrix in the interfacial transition zone is smaller at each distance than for the mortar. This is related to the fact that the mortar, at an equal volume fraction of aggregate, has a

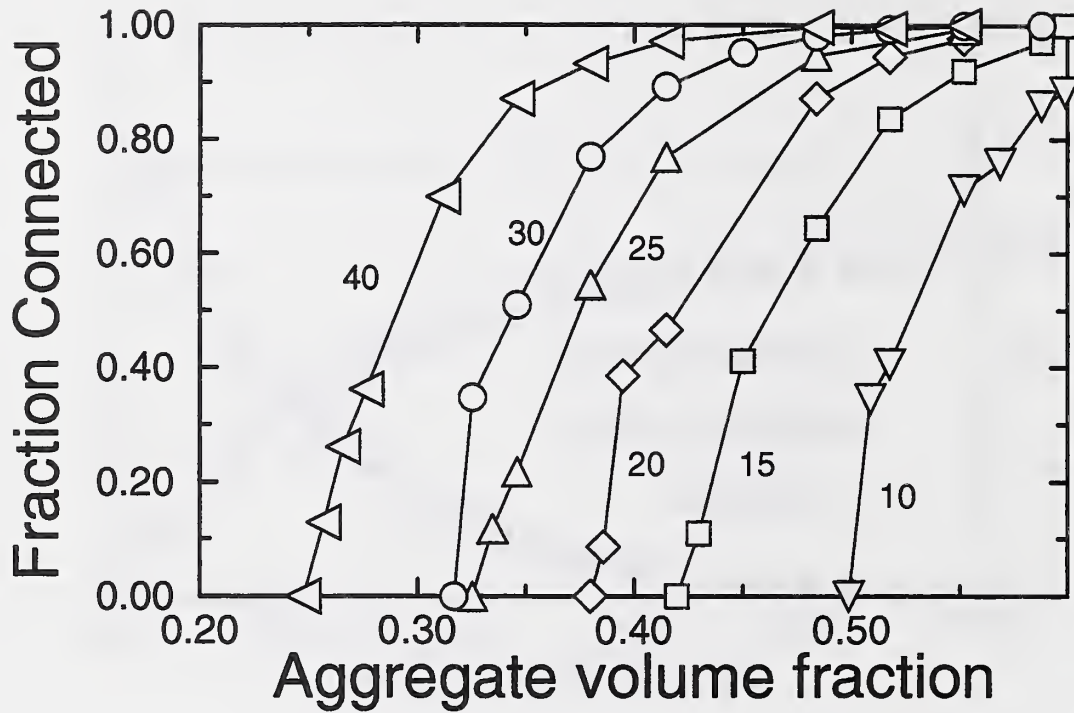


Figure 14: Showing the fraction of the total interfacial zone volume that is a part of a percolated (continuous) cluster as a function of aggregate volume fraction and for several interfacial zone thicknesses.

much larger surface area because of the smaller size of the aggregates, and therefore more interfacial transition zone material. This difference will also be reflected in the transport properties, as will be seen further below.

The interfacial transition zone percolation problem has also been studied for ellipsoidal aggregate particles [62] as a first look at how the aggregate shape could affect interfacial transition zone percolation. The aspect ratio of the ellipsoidal aggregates was varied between one and four, since most aggregates found in real concrete are reasonably spherical. The interfacial transition zone percolation threshold in terms of the aggregate volume fraction was found to be dependent on the aspect ratio of the aggregate. However, the interfacial transition zone percolation threshold in terms of the volume fraction of interfacial zone (paste) was not dependent on the aggregate aspect ratio [62].

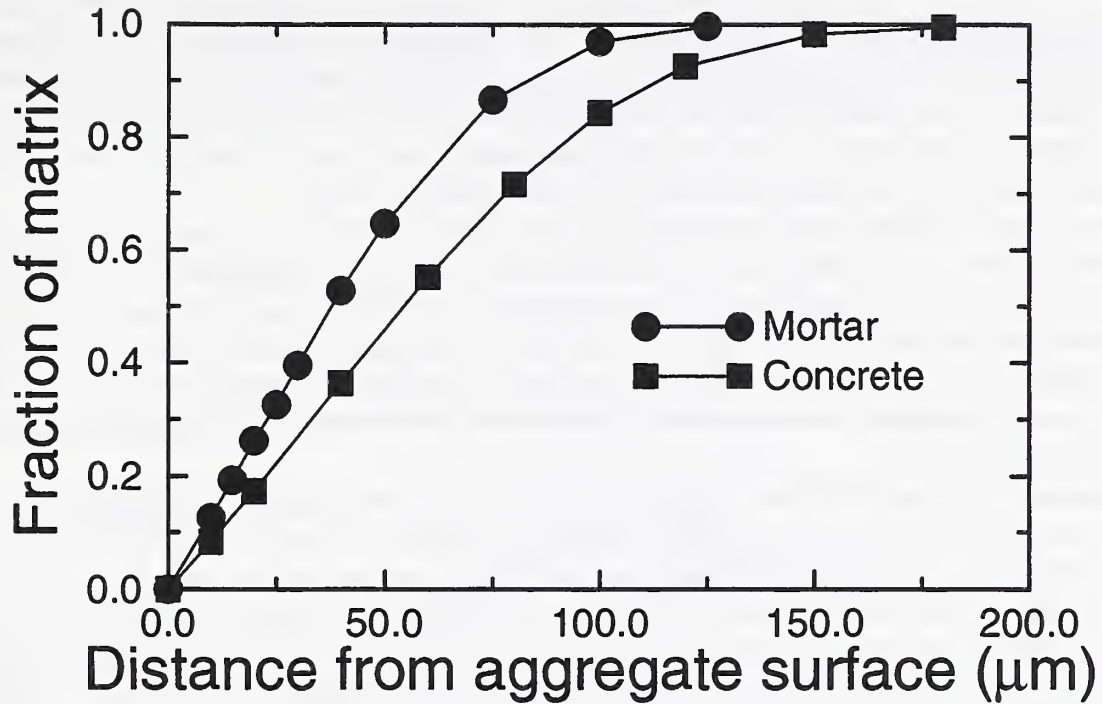


Figure 15: Showing the fraction of the total cement paste volume fraction that lies within a given distance from an aggregate surface, for a mortar with a sand volume fraction of 0.552, and a concrete with an aggregate volume fraction of 0.646.

#### 4.4 Diffusivity/conductivity of concrete

Concrete conducts electricity via the cement paste matrix, and the aggregates are assumed to be simply insulating obstacles to the flow of current. As was mentioned before, diffusivity is handled mathematically and physically the same way, so we specialize to conductivity language in the present discussion. Adapting the hard core/soft shell concrete model to study conductivity/diffusivity requires three input parameters: (1) the thickness of the interfacial layer, (2) the contrast in properties between this layer and the bulk cement paste, and (3) the concentration and size distribution of the aggregates. Following the previous discussion we will assume that all aggregates are spherical and that the interfacial transition zones are always spherical shells of constant thickness. As stated previously, while the thickness of the interfacial transition zone,  $h$ , may be as large as  $50\ \mu\text{m}$ , mercury intrusion measurements and modelling results [59] suggest that  $h = 20\ \mu\text{m}$  is a more typical value, especially since this is the main region having higher porosity and therefore higher conductivity. We assume

that the conductivity within the interfacial shell takes a constant value,  $\sigma_s$ , and that the conductivity of the cement paste,  $\sigma_p$ , is also constant. This is not, strictly speaking, quite true.

The actual situation is somewhat more complicated. Since the cement paste is mixed at a fixed w/c ratio, having extra porosity and thus extra water in the interfacial transition zone regions, which can occupy up to one third of the total matrix phase, means that the bulk paste must have a somewhat lower porosity and consequently a lower w/c ratio. Therefore, the conductivity of the matrix paste of a mortar or concrete cannot be simply taken as that of the cement paste from which the composite was made. Also, the interfacial transition zone region actually shows a gradient of properties, since it has a gradient in porosity [45]. The above model is still good, though, as a first approximation.

Since there is therefore no experimentally established value for the ratio  $\sigma_s/\sigma_p$ , we allow this parameter to vary freely in our calculations. For a given aggregate volume fraction, we have studied the dependence of the composite conductivity on the value of  $\sigma_s/\sigma_p$ . We have also studied the conductivity as a function of aggregate volume fraction for several fixed values of  $\sigma_s/\sigma_p$ . To compute the conductivity of such a model, we have adopted a random walk algorithm, used extensively in studies of disordered porous media and composite materials [71, 72, 73].

However, it is useful to first consider the limit of dilute aggregate concentration. The composite conductivity in this regime contains important information about the conductivity and size of the interfacial transition zone. This is the case because exact analytical calculations can be made of the influence of a small volume fraction of aggregates (each of which is surrounded by an interfacial shell) placed in a matrix. For the composite to be considered to be in the dilute limit, the volume fraction of aggregates must be small enough so that particles can be treated individually and do not affect each other. Consider mono-size spherical particles of conductivity  $\sigma_1$  and radius  $b$ , each surrounded by a concentric shell of thickness  $h$  and conductivity  $\sigma_2$ , and all embedded in a matrix of conductivity  $\sigma_3$ . If the volume fraction of sand grains is denoted by  $c$ , then the composite conductivity,  $\sigma$ , can be analytically approximated by an equation of the form  $\sigma/\sigma_3 = 1 + mc + O(c^2)$ , with  $m$  given by [61]:

$$m = \frac{3 \left[ (\sigma_1 - \sigma_2)(2\sigma_2 + \sigma_3) + \left( \frac{b+h}{b} \right)^3 (\sigma_1 + 2\sigma_2)(\sigma_2 - \sigma_3) \right]}{\left[ (\sigma_2 + 2\sigma_3)(\sigma_1 + 2\sigma_2) + 2 \left( \frac{b}{b+h} \right)^3 (\sigma_1 - \sigma_2)(\sigma_2 - \sigma_3) \right]} m_{def} \quad (1)$$

To make the connection to our mortar problem, let  $\sigma_1 = 0$ ,  $h$  = the interfacial zone thickness,  $\sigma_2 = \sigma_s$  (interfacial zone conductivity), and  $\sigma_3 = \sigma_p$  (bulk cement paste conductivity). For the random mortar model, or indeed for a real mortar, there is a size distribution of sand grain radii  $b_i$ , while the value of  $h$  is fixed. This implies that the slope  $m_i$  for each kind of particle will be a function of  $b_i$ , because the parameter  $[(b_i + h)/b_i]^3$  will be different for each particle. In a system with  $N$  different sand particle sizes, each with volume fraction  $c_i$ , the average slope  $\langle m \rangle$  is then defined by,

$$\langle m \rangle = \sum_{i=1}^N \frac{m_i c_i}{c} \quad (2)$$

where

$$\sum_{i=1}^N c_i = c \quad (3)$$

This dilute limit problem can also be solved in the case where a gradient of properties exists around the aggregate [74].

Using the four diameter model sand particle size distribution for a mortar mentioned previously [61], we can find the value of  $\langle m \rangle$  averaged over the appropriately-weighted four values of  $b_i$  [61]. Figure 16 shows a graph of this average slope  $\langle m \rangle$  as a function of  $\sigma_s/\sigma_p$ .

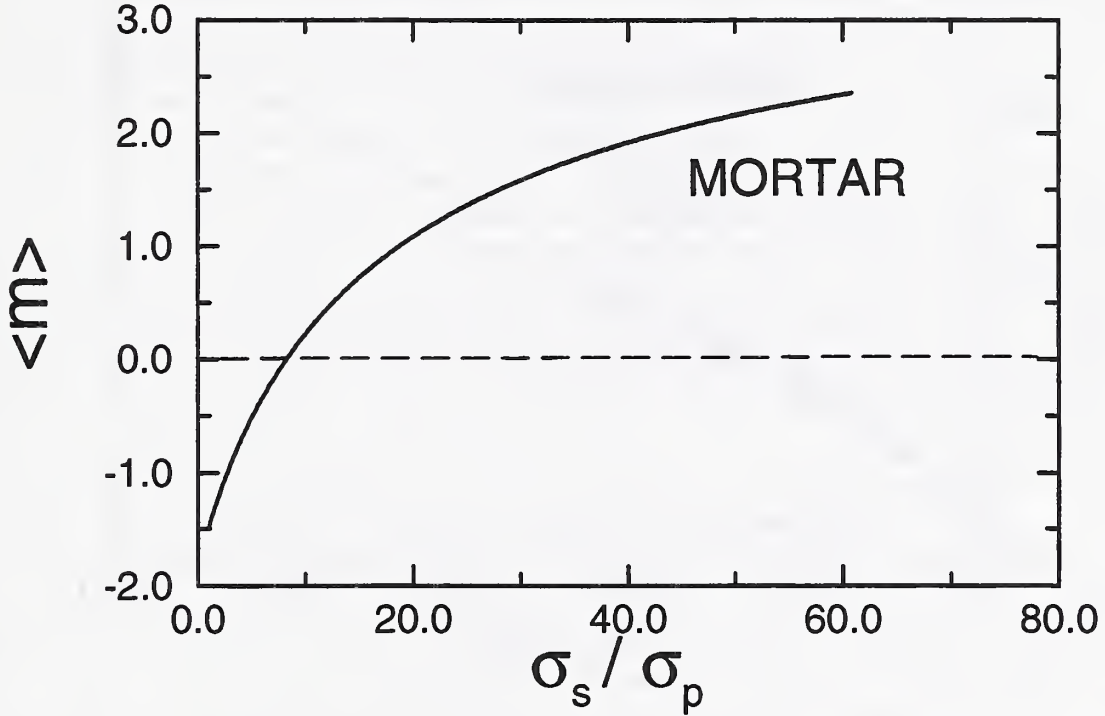


Figure 16: The exact initial slope of the conductivity, in the limit of dilute sand concentration, is shown as a function of  $\sigma_s/\sigma_p$  for the four size model mortar.

Note in the limit of  $\sigma_s/\sigma_p = 1$ , the slope  $\langle m \rangle = -3/2$ , which is the known exact result for insulating spherical inclusions of any size distribution [75]. The marked point on the graph is at  $\sigma_s/\sigma_p \approx 8.26$ , which is the point at which the slope  $\langle m \rangle = 0$ . At this value, to linear order in  $c$ , adding a few sand grains would have no effect on the overall conductivity.

Here one has a perfect balance between the negative influence of the insulating sand grains, and the positive effect of the enhanced conductivity in the interfacial shells.

The only exact results available for general three dimensional composite materials, in addition to the dilute limits presented above, are variational bounds [76]. However, effective medium theory (EMT) can often be employed to estimate composite properties at arbitrary volume fractions of the phases [77, 78]. By EMT we mean only those theories that properly describe the dilute limit, and are then built up via some sort of averaging assumption into approximate analytical equations. The two examples that have been previously considered are the self-consistent [77] and the differential [78] methods.

In Fig. 17 we present the random walk simulation results for the same four diameter aggregate mortar model together with the predictions of the differential (D-EMT) and self-consistent (SC-EMT) effective medium theories [66].

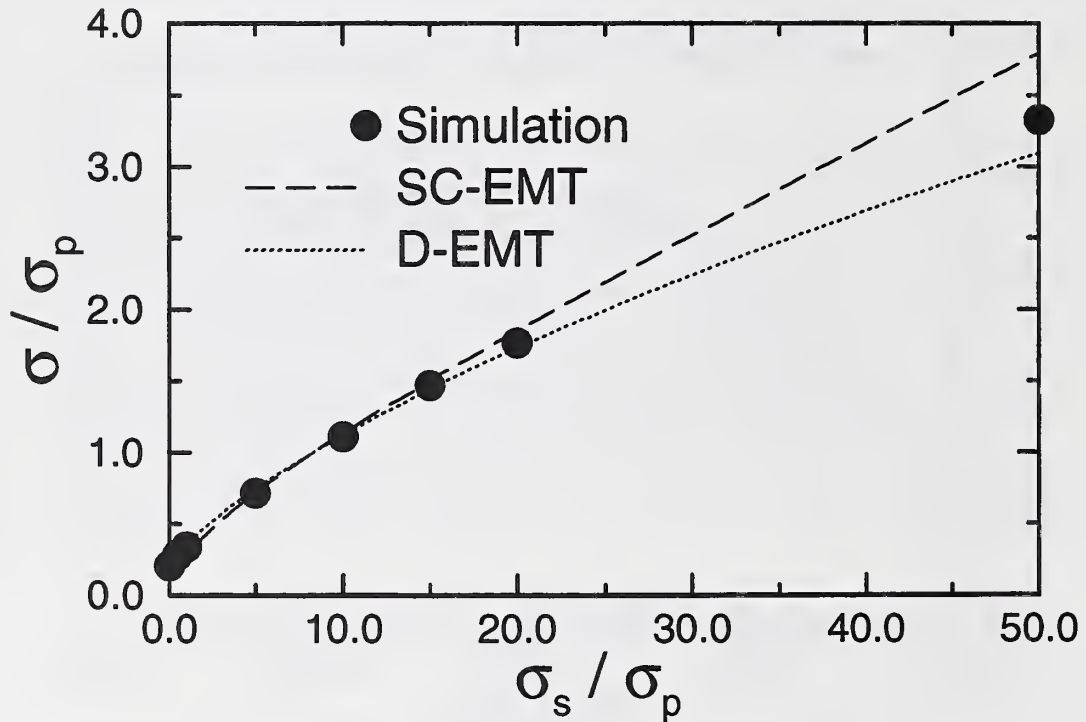


Figure 17: Composite conductivity for the four size model mortar is plotted vs. the interfacial zone conductivity. [Both are normalized by bulk paste conductivity.] The solid dots are the random walk data; also shown are the effective medium results (SC=self consistent and D=differential).

The simulations were of how the effective conductivity, at a single aggregate volume fraction, 55%, and a single interfacial transition zone thickness, 20  $\mu\text{m}$ , varied as a function of

the conductivity of the interfacial transition zone phase,  $\sigma_s$ , expressed as the dimensionless ratio  $\sigma_s/\sigma_p$ . The overall shape of the curves is concave down. In this case, the effective conductivity could at most be linear in  $\sigma_s/\sigma_p$ , for the following reason. If the two conducting phases, interfacial transition zone and bulk cement paste, were exactly in parallel geometrically, then the overall conductivity would be given by a simple linear combination of the two phase conductivities, and as  $\sigma_s$  increased, the overall conductivity would increase linearly. Since the microstructure is such that these two cement paste phases are not in parallel, the curve must be sub-linear, or concave down. As  $\sigma_s/\sigma_p \rightarrow \infty$  the curve will eventually become straight as predicted [61], since the interfacial transition zone conductivity will dominate the effective conductivity. Note that by the point that  $\sigma_s/\sigma_p = 20$ , the effective conductivity is almost double the pure matrix conductivity,  $\sigma/\sigma_p \approx 1.8$ .

The data in Fig. 17 indicate that to achieve an overall conductivity that is equal to the bulk cement paste conductivity, the value of  $\sigma_s/\sigma_p$  must be equal to approximately 8. This is remarkably close to the dilute limit result  $\sigma_s/\sigma_p \approx 8.26$  found in Fig. 16. Because the dilute limit seems to define an essential feature of the overall curve, effective medium theories that are based on the dilute limit have a good possibility of successfully predicting the essential structure of the composite conductivity. The two EMT's displayed in Fig. 17 do show reasonably good agreement with the simulation data.

Figure 18 shows computed conductivity data for the random mortar model as a function of sand volume fraction, for  $\sigma_s/\sigma_p = 20, 5$ , and 1.

The curve for  $\sigma_s/\sigma_p = 20$  is concave up, with an initial slope that is positive, since  $\sigma_s/\sigma_p = 20 > 8.26$ . Both EMT's predict that when the initial slope is positive, the value of the effective conductivity,  $\sigma/\sigma_p$ , will always be greater than 1. The simulation data do obey this prediction. The value of  $\sigma_s/\sigma_p = 20$  is not high enough in order to see clear evidence of the interfacial zone percolation threshold, which, for much higher values of  $\sigma_s/\sigma_p$ , would manifest itself as a sharply increasing conductivity near the percolation threshold. The  $\sigma_s/\sigma_p = 5$  and 1 curves have negative initial slopes, and the effective conductivities remain below one, as predicted also by EMT. The  $\sigma_s/\sigma_p = 1$  curve roughly follows a  $3/2$  power law in the total cement paste volume fraction, as would be expected since there is no difference between interfacial zone and bulk cement paste in this case [75].

Figure 19 shows analytical results for  $\langle m \rangle$  for a typical mortar [79] and a typical concrete [67]. At a given value of  $\sigma_s/\sigma_p$ , the value of  $\langle m \rangle$  for the mortar is always higher than that for the concrete. This comes back to the same point made earlier, that the mortar has a larger surface area at a given volume fraction, due to the smaller average particle size, and so the interfacial zone has a larger volume and plays a bigger role in its composite properties than it does in the concrete's composite properties.

## 5 C-S-H

The C-S-H phase plays the role as the glue that holds cement paste together. We now go down from the micrometer length scale of cement paste and the millimeter scale of concrete, to examine models for the structure of the nanometer-scaled C-S-H phase. Little is known of the actual details of the atomic structure of C-S-H, as it is amorphous, so the model focuses on the nanometer scale.

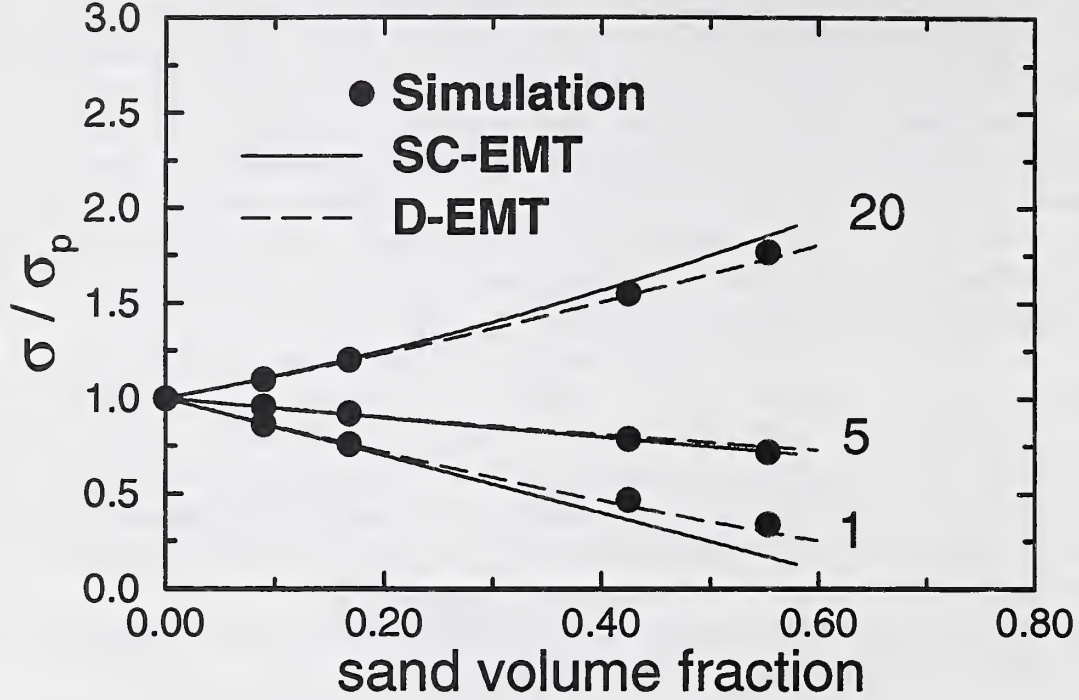


Figure 18: Composite conductivities (calculated by random walk simulations) for the random model are shown as a function of sand concentration for three values of the interfacial zone conductivity. Also shown are the predictions of the SC and D-EMT calculations, with the same normalization as in the previous figure.

At the scale of nanometers, the C-S-H gel is modelled as a two-level structure of partially overlapping spherical particles [80]. At the macro level, the 2-D cross-section of the larger 40 nm spherical agglomerates shown in the righthand image of Fig. 20 are each composed of smaller 5 nm diameter micro level particles, as shown in the lefthand image of Fig. 20.

The particle sizes and the total porosity at each level have been chosen to be consistent with experimental data from small angle neutron scattering [6] and sorption measurements [81]. The models are generated in continuum space (in a three-dimensional cube with periodic boundaries) and subsequently digitized into a 3-D digital image for the evaluation of properties. The structural models have been validated by computing sorption isotherms and the pore volume accessible to molecules of varying diameters, and comparing to experimental results [80]. Computational techniques have also been applied to computing both the conductivity/diffusivity and the permeability [20] of the macro-level gel structure, with reasonable agreement with experiment.

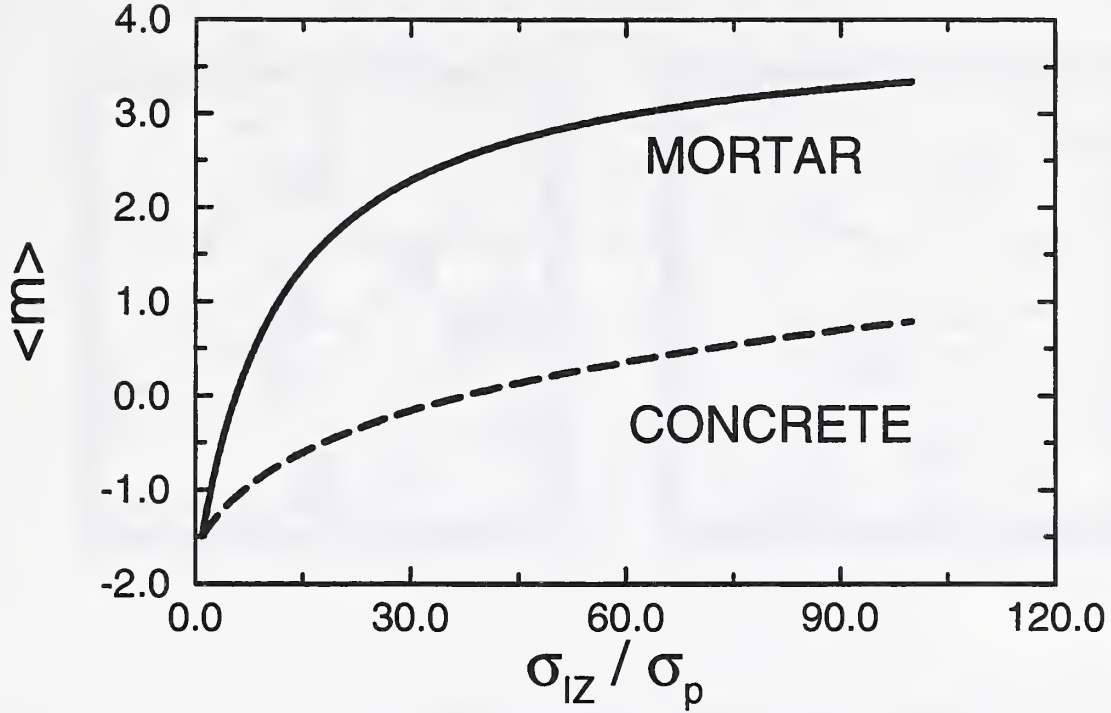


Figure 19: The exact initial slope of the conductivity, in the limit of dilute sand concentration, is shown as a function of  $\sigma_s/\sigma_p$  for a typical mortar and a typical concrete aggregate particle size distribution.

## 6 Multiscale models for the ionic diffusivity

As has been mentioned earlier, computer modelling of the properties and performance of cement-based materials is complicated by the large range of relevant size scales. Processes occurring in the nanometer-sized pores ultimately affect the performance of these materials at larger length scales. At present, it is impossible to simultaneously handle all these length scales, from nanometers to millimeters and larger, using a single computer-based model. One approach to alleviating this complication is the development of a suite of models, consisting of individual digital-image-based or continuum structural models for the calcium silicate hydrate gel at the nanometer level, the hydrated cement paste at the micrometer level, and a mortar or concrete at the millimeter level. Computations performed at one level provide input properties to be used in simulations of performance at the next higher level. This is the ultimate goal of this research, and will be demonstrated for the property of ionic diffusivity in saturated concrete, using the models discussed in previous sections. Here the relative diffusivity of concrete is computed. The relative diffusivity is defined as the ratio

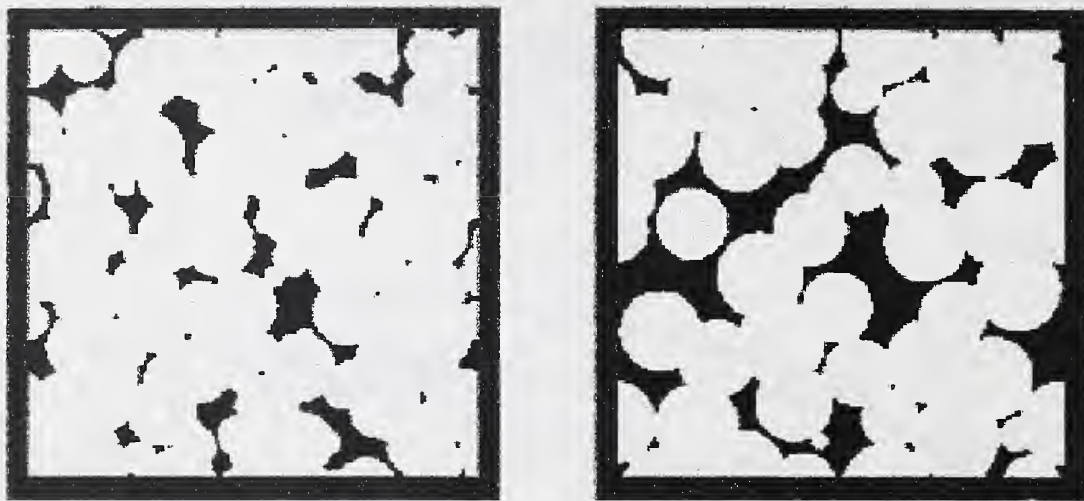


Figure 20: Two-dimensional slices from three-dimensional model microstructures of the C-S-H gel at the scale of nanometers. The left image is of the micro model (25 nm by 25 nm), and the right image is of the macro model (250 nm by 250 nm). White=solid, black=pore.

of the diffusivity of ions in a composite medium to their diffusivity in bulk water. Based on the Nernst-Einstein relation, the relative diffusivity  $D/D_o$  is equivalent to the relative conductivity  $\Gamma = \sigma/\sigma_o$ . In this case, saturated means that all the pore space is filled with the same pore fluid.

The Nernst-Einstein equation is used to determine the diffusivity by solving the equivalent electrical problem for the electrical conductivity of the composite material [30]. As was discussed above, to solve for the properties of these models, the properties of each phase in a microstructure must be known or assumed. The multiscale approach we use is to utilize properties computed at one scale level of modelling as input into the computation procedures employed at a higher scale. For example, the conductivity/diffusivity computed for the C-S-H gel nanostructure model can be used as an input property into the cement paste microstructure model, so that the conductivity/diffusivity of cement paste can be computed as a function of  $w/c$  and  $\alpha$ . Likewise, the diffusivity computed for bulk and interfacial transition zone cement paste can be used in the model of concrete at the level of millimeters, to compute the diffusivity of a concrete, the quantity of actual interest to a design or structural engineer.

The first step is the computation of the relative diffusivity of the C-S-H gel. Using the electrical analogy and the nanostructural model shown in the top portion of Fig. 20, a value of  $1/300$  is computed for the relative diffusivity of the gel. Here, we assume that diffusive

transport occurs only in the cluster-level pores and not in the much smaller pores shown in the particle-level model in the top portion of Fig. 20. This is a reasonable assumption, since these smaller, nanometer size pores are on the order of the size of a water molecule and would be virtually inaccessible to many diffusing ions. A further assumption is that this relative diffusivity value is characteristic of all C-S-H gel regardless of cement composition or when during the hydration process the C-S-H is produced. When trying to match simulation results for the ionic diffusivity of cement paste to experimental results by adjusting the value of the relative diffusivity assigned to the C-S-H phase, we found a value of approximately  $1/400$  [30], so reasonably good agreement, albeit in an indirect way, has been obtained for the nanometer-scale model.

The second step is to use the value computed for the relative diffusivity of the C-S-H gel in a computation of the relative diffusivity of cement pastes of various w/c ratios and degrees of hydration. A diffusivity value of 1.0 is assigned to the capillary porosity, while the unhydrated cement and calcium hydroxide are assigned diffusivities of 0.0 since they contain no porosity. Again using the electrical analogy, computations performed for a variety of  $100^3$  element microstructures have resulted in the development of an equation which relates relative diffusivity to the capillary porosity of the cement paste. Good agreement has been observed in comparing these computed model values to ones measured experimentally both for chloride ion diffusivity [29, 34] and cement paste conductivity [28].

Finally, the relative diffusivity values computed for cement paste can be used as input into the structural model for mortar to determine the effect of aggregates and their surrounding interfacial zones on the diffusivity of the mortar,  $D_M$ . At this level, one must select the thickness of the interfacial zone paste and the value of its diffusivity  $D_{ITZ}$  compared to that of the bulk paste  $D_P$ . Techniques like those described in Refs. [61, 66] can then be used to compute  $D_M$ . Care must be taken to properly allow for the redistribution of cement between the interfacial transition zone regions and the bulk cement paste. For a given w/c cement paste surrounding the aggregate grains, higher porosity in the interfacial transition zone region means a lower porosity in the bulk cement paste regions. This redistribution of cement determines the correct ratio of diffusivities that is needed to be used in the models of Refs. [61, 66]. A technique that approximately allows for this redistribution has been described [74, 83, 84].

## 7 Summary

It has been shown that theoretical understanding of the microstructure:transport property relationships of concrete, from the cement paste up to the full composite, can be based on the ideas of pore size and connectivity, with connectivity defined rigorously using percolation concepts. These concepts give a fairly complete, although at present mainly qualitative, picture of how transport properties depend on microstructure in concrete. Percolation phenomena in concrete include the setting of cement paste, the connectivity of the C-S-H gel phase, the disconnection of the capillary pore space in cement paste, the effect of leaching of calcium hydroxide on the transport properties of cement paste, and the connection of the interfacial transition zones in concrete. Like the material itself, percolation phenomena are important over many length scales, and since more than one phase of the concrete composite

is simultaneously percolated, concrete must be considered to be an interpenetrating phase composite [81].

The use of a set of multi-scale microstructure models to investigate transport and mechanical properties of concrete has been demonstrated. By relating microstructure to properties at all relevant size scales, a more complete understanding of the influence of microstructure and the underlying physical processes on the performance of these composite materials can be obtained. For the case of chloride diffusivity, a nearly complete set of results has been presented [83, 84]. As the structural modelling and computational capabilities described herein continue to evolve, their use as a tool in the design of a concrete with desired properties and service life should become a reality.

## 8 Acknowledgements

The authors thank the High Performance Construction Materials and Systems program at NIST and the National Science Foundation Science and Technology Center for Advanced Cement-Based Materials for partial funding of this work. We also thank our many collaborators in this research, whose names are listed throughout the references.

## 9 References

- [1] F.M. Lea, *The Chemistry of Cement and Concrete* (St. Martin's Press, New York, 1956), Chapter 1.
- [2] J.F. Young, A Review of the Pore Structure of Cement Paste and Concrete and Its Influence on Permeability, in *Permeability of Concrete*, ed. by D. Whiting and A. Walitt, ACI SP-108 (American Concrete Institute, Detroit, 1988).
- [3] E.J. Garboczi, Computational materials science of cement-based materials, *Materials and Structures* **26**, 191-195 (1993).
- [4] H.F.W. Taylor, *Cement Chemistry* (Academic Press, San Diego, 1990).
- [5] R. Maggion, PhD thesis, L'Universit D'Orleans, France 1992.
- [6] A.J. Allen, R.C. Oberthur, D. Pearsons, P. Schofield, and C.R. Wilding, Development of the fine porosity and gel structure of hydrating cement systems, *Philosophical Magazine B* **56**, No. 3, pp. 263-288 (1987).
- [7] E.J. Garboczi, M.F. Thorpe, M. DeVries, and A.R. Day, Universal Conductivity Curve for a Plane Containing Random Holes, *Physical Review A* **43**, 6473-6482 (1991).
- [8] E.J. Garboczi, K.A. Snyder, J.F. Douglas, and M.F. Thorpe, Geometrical percolation threshold of overlapping ellipsoids, *Phys. Rev. E* **52**, 819-828 (1995).
- [9] a) J. Kertesz, *J. Phys. Lett. (Paris)* **42**, L393 (1981), b) W.T. Elam, A.R. Kerstein, and J.J. Rehr, *Phys. Rev. Letts.* **52**, 1516 (1984), c) S.B. Lee and S. Torquato, Porosity for the penetrable-concentric-shell model of two-phase disordered media: Computer simulation results, *J. Chem. Phys.* **89**, 3258 (1988).
- [10] D.P. Bentz and P.E. Stutzman, SEM Analysis and Computer Modelling of Hydration of Portland Cement Particles, in *ASTM STP 1215*, ed. S.M. DeHayes and D. Stark (American Society for Testing and Materials, Philadelphia, 1994), 60-73.
- [11] *High-Performance Construction Materials and Systems: An Essential Program for America and Its Infrastructure*, Technical Report 93-5011 (Civil Engineering Research Foundation, Washington, D.C., 1993).
- [12] D.P. Bentz, P.V. Coveney, E.J. Garboczi, M.F. Kleyn, and P.E. Stutzman, Cellular automaton simulations of cement hydration and microstructure development, *Modelling and Simulation in Materials Science and Engineering* **2**, 783-808 (1994).
- [13] D.P. Bentz, and E.J. Garboczi, *Guide to Using HYDRA3D: A Three-Dimensional Digital-Image-Based Cement Microstructure Model* NISTIR 4746, U.S. Department of Commerce (1992).
- [14] Wei-Guo Lei, *Rheological studies and percolation modelling of microstructure development of fresh cement paste*, Ph.D. Thesis, University of Illinois, Department of Materials Science and Engineering, 1995.

- [15] Y. Chen and I. Odler, On the Origin of Portland Cement Setting, *Cem. Conc. Res.* 22, 1130-1140 (1992).
- [16] ASTM C-191 (1992) Standard Test Method for Time of Setting of Hydraulic Cement by Vicat Needle, American Society for Testing of Materials, Philadelphia, Pa.
- [17] C.M. Sayers and R.L. Grenfell, Ultrasonic propagation through hydrating cements, *Ultrasonics* **31**, 147-153 (1993).
- [18] S.P. Jiang, J.C. Mutin, and A. Nonat, Analysis of the Hydration Setting Relation: Towards a Comprehensive Approach to Cement Setting, in *Proceedings of the 9th International Congress on the Chemistry of Cement, Vol. III*, 17-23, New Delhi, India.
- [19] D.P. Bentz and E.J. Garboczi, Percolation of Phases in a Three-Dimensional Cement Paste Microstructural Model, *Cem. and Conc. Res.* 21, 325-344 (1991).
- [20] D.P. Bentz, E.J. Garboczi, and N.S. Martys, Application of digital-image-based models to microstructure, transport properties, and degradation of cement-based materials, in *Proceedings of 1994 NATO/RILEM Workshop Computer Modelling of Microstructure and Its Potential Application to Transport Properties*, edited by H.M. Jennings, pp. 167-186.
- [21] R.T. Coverdale, *Microstructural analysis of cement paste using a computer model of impedance spectroscopy*, Ph.D. thesis, Northwestern University, Department of Materials Science and Engineering, 1993.
- [22] C. Legrand and E. Wirquin, Effects of the initial structure of the cement paste in fresh concrete on the first developments of strength, in *Proceedings of the 9th International Congress on the Chemistry of Cement*, vol V, 95-99, New Delhi, India (1992).
- [23] S.P. Jiang, J.C. Mutin, and A. Nonat, Effect of melment superplasticizer on C3S hydration: From suspension to paste, in *Proceedings of the 3rd Beijing International Symposium on Cement and Concrete*, China Building Materials Academy, 126-131 (1993).
- [24] W.G. Lei, L.J. Struble, D.P. Bentz, E. Schlangen, and E.J. Garboczi, in preparation.
- [25] T.C. Powers, L.E. Copeland, and H.M. Mann, *PCA Bulletin* **10** (1959).
- [26] D.P. Bentz, unpublished.
- [27] B.J. Christensen, T.O. Mason, and H.M. Jennings, Influence of silica fume on the early hydration of portland cement pastes using impedance spectroscopy, *Journal of the American Ceramic Society* **75**, 935-939 (1992).
- [28] R.A. Olson, B.J. Christensen, R.T. Coverdale, S.J. Ford, G.M. Moss, H.M. Jennings, T.O. Mason, and E.J. Garboczi, "Interpretation of the impedance spectroscopy of cement paste via computer modelling III: Microstructural analysis of frozen cement paste, *Journal of Materials Science* **30**, 5078-5086 (1995).

- [29] P. Halamickova, R.J. Detwiler, D.P. Bentz, and E.J. Garboczi, "Water Permeability and Chloride Ion Diffusion in Portland Cement Mortars: Relationship to Sand Content and Critical Pore Diameter, *Cem. and Conc. Res.* **25**, 790-802 (1995).
- [30] E.J. Garboczi and D.P. Bentz, Computer Simulation of the Diffusivity of Cement-Based Materials, *J. Mater. Sci.* **27**, 2083-2092 (1992)
- [31] A. Atkinson and A.K. Nickerson, *J. Mater. Sci.* **19**, 3068 (1984).
- [32] R.T. Coverdale, B.J. Christensen, H.M. Jennings, T.O. Mason, D.P. Bentz, and E.J. Garboczi, Interpretation of the impedance spectroscopy of cement paste via computer modelling I: Bulk conductivity and offset resistance, *Journal of Materials Science* **30**, 712-719 (1995).
- [33] R.T. Coverdale, B.J. Christensen, T.O. Mason, H.M. Jennings, and E.J. Garboczi, Interpretation of the impedance spectroscopy of cement paste via computer modelling II: Dielectric response, *Journal of Materials Science* **29**, 4984-4992 (1994).
- [34] B.J. Christensen, T.O. Mason, H.M. Jennings, D.P. Bentz, and E.J. Garboczi, Experimental and computer simulation results for the electrical conductivity of portland cement paste, in *Advanced Cementitious Systems: Mechanisms and Properties*, **245**, 259-264 (Materials Research Society, Pittsburgh, 1992).
- [35] B.J. Christensen, *Microstructure studies of hydrating portland cement-based materials using impedance spectroscopy*, Ph.D. thesis, Northwestern University, Department of Materials Science and Engineering, 1993.
- [36] B.J. Christensen, T.O. Mason, R.T. Coverdale, H.M. Jennings, R.A. Olson, and E.J. Garboczi, Impedance spectroscopy and the electrical properties of hydrating cement-based materials: A review, *Journal of the American Ceramic Society* **77**, 2789-2804 (1994).
- [37] D.P. Bentz and E.J. Garboczi, Modelling the leaching of calcium hydroxide from cement paste: Effects on pore space percolation and diffusivity, *Materials and Structures* **25**, 523-533 (1992).
- [38] E. Revertegat, C. Richet, and P. Gegout, Effect of pH on the durability of cement pastes, *Cem. and Conc. Res.* **22**, 259-272 (1992).
- [39] P.K. Mehta and P.J.M. Monteiro, *Concrete: Structure, Properties, and Materials* (Prentice-Hall, Englewood Cliffs, New Jersey, 1993).
- [40] D.P. Bentz, E. Schlangen, and E.J. Garboczi, in *Materials Science of Concrete IV*, edited by J.P. Skalny and S. Mindess (American Ceramic Society, Westerville, OH, 1994), 155-200.
- [41] S. Diamond, S. Mindess, and J. Lovell, pp. C42 in *Liasons Pater de Ciment Materiaux Associes*, RILEM, Toulouse, France, 1982.

- [42] D.P. Bentz, N.S. Martys, P.E. Stutzman, M.S. Levenson, E.J. Garboczi, J. Dunsmuir, and L.M. Schwartz, X-Ray Microtomography of an ASTM C109 Mortar Exposed to Sulfate Attack, in *Microstructure of Cement-Based Systems/Bonding and Interfaces in Cementitious Materials* (Materials Research Society, Pittsburgh, 1995), 77-82.
- [43] J. Farran, *Rev. Mater. Const.* **490-491**, 155-172 (1956).
- [44] J.C. Maso, in *Proc. 7th Intl. Cong. on Chem. of Cement*, Paris, 3-15 (1980).
- [45] Karen Scrivener, The Microstructure of Concrete, in *Materials Science of Concrete I*, ed. by Jan Skalny (American Ceramic Society, Westerville, 1990).
- [46] E.J. Garboczi and D.P. Bentz, Digital simulation of the aggregate-cement paste interfacial zone in concrete, *Journal of Materials Research* **6**, 196-201 (1991).
- [47] D.P. Bentz, E.J. Garboczi, and P.E. Stutzman, Computer Modelling of the Interfacial Zone in Concrete, in *Interfaces in Cementitious Composites*, ed. by J. Maso (E and FN Spon, London, 1992), 107-116.
- [48] D.P. Bentz and E.J. Garboczi, Simulation Studies of the Effects of Mineral Admixtures on the Cement Paste-Aggregate Interfacial Zone, *American Concrete Institute Materials Journal* **88**, 518-529 (1991).
- [49] Z. Hashin, Analysis of Composite Materials: A Survey, *Journal of Applied Mechanics* **50**, 481-505 (1983).
- [50] C.L. Page and V.T. Ngala, in *Proceedings of Conference on Chloride Diffusivity in Concrete*, RILEM, France (1995).
- [51] J. Ollivier, *J. of Adv. Cement-Based Mater.*, in press (1996).
- [52] Y.F. Houst, H. Sadouki, and F.H. Wittmann, Influence of aggregate concentration on the diffusion of CO<sub>2</sub> and O<sub>2</sub>, in *Interfaces in Cementitious Composites*, ed. by J. Maso (E and FN Spon, London, 1992), 279-288.
- [53] R.W. Zimmerman, M.S. King, and P.J. M. Monteiro, *Cem. Con. Res.* **16**, 239 (1986).
- [54] A. Ulrik Nilsen and P.J.M. Monteiro, Concrete: A Three Phase Material, *Cem. and Conc. Res.* **23**, 147-151 (1993).
- [55] M.D. Cohen, A. Goldman, and W.F. Chen, The role of silica fume in mortar: Transition zone versus bulk paste modification, *Cem. and Conc. Res.* **24**, 95-98 (1994).
- [56] K.A. Snyder and J.R. Clifton, Measures of air void spacing, in *Proceedings of the International Conference on Building Materials*, Weimar, Germany, 155-157 (1994).
- [57] K.A. Snyder, J.R. Clifton, and L.I. Knab, Freeze-thaw susceptibility of high performance concrete, in *Proceedings of the International Conference on Building Materials*, Weimar, Germany, 139-142 (1994).

- [58] A.I. Rashed and R.B. Williamson, *Journal of Materials Research* **6**, 2004-2012 (1991).
- [59] D.N. Winslow, M. Cohen, D.P. Bentz, K.A. Snyder, and E.J. Garboczi, Percolation and porosity in mortars and concretes, *Cem. and Conc. Res.* **24**, 25-37 (1994).
- [60] S. Torquato, *J. Chem. Phys.* **85**, 6248 (1986).
- [61] E.J. Garboczi, D.P. Bentz, and L.M. Schwartz, Modelling the influence of the interfacial zone on the D.C. electrical conductivity of mortar, *Journal of Advanced Cement-Based Materials* **2**, 169-181 (1995).
- [62] D.P. Bentz, J.T.G. Hwang, C. Hagwood, E.J. Garboczi, K.A. Snyder, N. Buenfeld, and K.L. Scrivener, Interfacial Zone Percolation in Concrete: Effects of Interfacial Zone Thickness and Aggregate Shape, in *Microstructure of Cement-Based Systems/Bonding and Interfaces in Cementitious Materials* (Materials Research Society, Pittsburgh, 1995), 437-442.
- [63] G. E. Pike and C. H. Seager, *Phys. Rev. B* **10**, 1421 (1974).
- [64] A.L. Bug, S.A. Safran, G.S. Grest, and I. Webman, *Phys. Rev. Letts.* **55**, 1896 (1985).
- [65] D. W. Cooper, *Phys. Rev. A* **38**, 522 (1988).
- [66] L.M. Schwartz, E.J. Garboczi, and D.P. Bentz, Interfacial transport in porous media: Application to D.C. electrical conductivity, *Journal of Applied Physics* **78**, 5898-5908 (1995).
- [67] D. Winslow and D. Liu, *Cem. and Conc. Res.* **20**, 227-234 (1990).
- [68] K.A. Snyder, D.N. Winslow, D.P. Bentz, and E.J. Garboczi, Effects of Interfacial Zone Percolation on Cement-Based Composite Transport Properties, in *Advanced Cementitious Systems: Mechanisms and Properties*, ed. by F.P. Glasser, G.J. McCarthy, J.F. Young, T.O. Mason, and P.L. Pratt (Materials Research Society, Pittsburgh, 1992), 265-270.
- [69] K.A. Snyder, D.P. Bentz, E.J. Garboczi, and D.N. Winslow, Interfacial zone percolation in cement-aggregate composites, in *Interfaces in Cementitious Composites*, ed. by J. Maso (E and FN Spon, London, 1992), 259-268.
- [70] D.N. Winslow and S. Diamond, *ASTM J. of Materials* **5**, 564 (1970).
- [71] L.M. Schwartz and J.R. Banavar, *Phys. Rev. B* **39**, 11965-11970 (1989).
- [72] I.C. Kim and S. Torquato, *Phys. Rev. A* **43**, 3198 (1991).
- [73] D.C. Hong, H.E. Stanley, A. Coniglio, and A. Bunde, *Phys. Rev. B* **33**, 4564 (1986).
- [74] E.J. Garboczi and D.P. Bentz, "The effect of the interfacial transition zone on concrete properties: The dilute limit," November, 1996 Amer. Soc. Civil Eng. 4th Materials Conference, Washington, DC.

- [75] R.E. De La Rue and C.W. Tobias, J. Electrochemical Soc. **106**, 827 (1959).
- [76] S. Torquato, Appl. Mech. Rev. **44**, 37 (1991).
- [77] Z. Hashin, J. Composite Mater. **2**, 284 (1968).
- [78] McLaughlin, Int. J. Eng. Sci. **15** , 237 (1977).
- [79] ASTM Standard C-109, in *ASTM Annual Book of Standards 04.01: Cement; Lime; Gypsum* (ASTM, Philadelphia, 1995).
- [80] D.P. Bentz, D.A. Quenard, V. Baroghel-Bouny, E.J. Garboczi, and H.M. Jennings, Modelling drying shrinkage of cement paste and mortar Part 1: Structural models from nanometers to millimeters, *Materials and Structures* **28**, 450-458 (1995).
- [81] Baroghel-Bouny, V., PhD thesis, L'ecole Nationale des Ponts et Chaussees, France 1994.
- [82] D.R. Clarke, Interpenetrating Phase Composites, J. Am. Ceram. Soc. **75**, 739-759 (1992).
- [83] D.P. Bentz, E.J. Garboczi, and E.S. Lagergren, Multi-scale microstructural modelling of concrete diffusivity: Identification of significant variables, submitted to ASTM Cement and Aggregates.
- [84] E.J. Garboczi and D.P. Bentz, Multi-scale analytical/numerical theory of the diffusivity of concrete, submitted to J. of Adv. Cem.-Based Mater.



